in the spinal cord. The injury was so severe that the lesion core, which was filled with collagen IV 1 week after injury, occupied a significant area of the spinal cord (data not shown). The injury sizes estimated by collagen IV or GFAP staining did not vary between individual rats (data not shown).

Disulfated KS contents in the injured region increased after injury, peaking at 7 d (Fig. 1*A*). CS-C contents also increased, peaking at ~7 d after injury (Fig. 1*B*), consistent with a previous report (Properzi et al., 2005).

K-II (0.05 U) or C-ABC (0.05 U) was then locally administered to the injured site for 2 weeks after contusion injuries using an osmotic pump. Disulfated KS contents decreased to the non-injury level after K-II treatment (Fig. 1*A*). Western blot and immunohistochemical analyses revealed that the reactivity to KS antibody 5D4 was lost in rats treated with K-II for 7 d after injury, but not in C-ABC-treated rats (Fig. 1*C*,*D*). The smear appearance in Western blot is probably due to the long sugar chains, and is the nature of proteoglycans. The granular staining profile in Figure 1*D* represented the main source of KS expression, i.e., microglia (Fig. 1*E*), which is consistent with previous reports (Jones and Tuszynski, 2002; Ito et al., 2010). As disulfated KS was still detected after K-II treatment by disaccharide analysis using HPLC (Fig. 1*B*), the almost complete disappearance of KS in Western blot and immunohistochemistry may be due to the limited ability of the 5D4 antibody to detect KS.

To detect diffusion of infused enzyme, biotin-labeled K-II was infused and detected by immunohistochemistry. We found that the enzyme diffused to cover the most area of injury, but did not cover the whole spinal cord (supplemental Fig. 2, available at www.jneurosci.org as supplemental material). These data collectively demonstrated that K-II worked well *in vivo*, although it did not completely abolish KS.

The *in vivo* degradation of CS by C-ABC, but not that by K-II, was also confirmed by HPLC analysis (Fig. 1*B*) and Western blot analysis (Fig. 1*C*).

Motor function recovery by K-II

We next evaluated motor function recovery using the BBB score and %grip test. K-II led to a striking recovery of motor function; the effect was similar to that of C-ABC (Fig. 2*A*,*B*; supplemental Tables 1, 2, available at www.jneurosci.org as supplemental material). There was no significant difference in motor function between the K-II- and C-ABC-treated groups (Fig. 2*A*,*B*). The observed motor function recovery was confirmed by an electrophysiological technique, motor-evoked potential (MEP) monitoring, in which an electric stimulus is given at the thoracic level (Th7), and a response is taken at the gastrocnemius muscles (Fig. 2*C*; supplemental Table 3, available at www.jneurosci.org as supplemental material). K-II also showed significant functional recovery after SCI even at lower doses, e.g., as low as 2000× dilution (Fig. 2*D*; supplemental Table 4, available at www.jneurosci.org as supplemental material). No significant differences were observed between the K-II-, K-II (10× dilution)-, and K-II (2000× dilution)-treated groups (Fig. 2*D*). Consistent with this finding, K-II and K-II (2000× dilution) decreased disulfated KS contents in the spinal cord to similar extents (Fig. 1*A*). This functional recovery was due to the enzymatic activity of K-II, as heat-inactivated K-II did not promote motor function recovery at all (Fig. 2*E*; supplemental Table 4, available at www.jneurosci.org as supplemental material).

Interestingly, even though K-II or C-ABC treatment promoted the recovery of motor function, the combination of these two enzymes showed neither additive nor synergistic effects (Fig. 2*C*,*F*; supplemental Tables 3, 5, available at www.jneurosci.org as supplemental material).

Sensory function recovery by K-II

SCI induced thermal hyperalgesia and mechanical allodynia (Fig. 3*A*,*B*). The tail-immersion test and touch test showed that thermal hyperalgesia and mechanical allodynia were ameliorated by K-II or C-ABC treatment, reaching an almost normal level 10 weeks after injury (Fig. 3*A*,*B*). sp-SCEP, in which an epidural electric stimulus was given at the Th11 level and a response was taken at the Th7 level, was performed 8 weeks after injury. The results of this test support the idea that the sensory function was recovered by K-II or C-ABC treatment (Fig. 3*C*). The reinjury of K-II-treated rats lost the recovered response of sp-SCEP (Fig. 3*C*), and the results were consistent with those of previous reports (Rapalino et al., 1998; Bradbury et al., 2002).

As seen in motor function recovery, the combination of K-II and C-ABC showed neither additive nor synergistic effects on sensory function recovery (Fig. 3*C*,*D*).

Histological analysis of functional recovery after SCI

We reconstructed the serial section of the spinal cord using all of the 50–60 serial longitudinal sections per rat and estimated the number of fibers strained for GAP-43 or 5-HT. The GAP-43 and 5-HT data from the vehicle and treated groups were compared with sham-lesioned controls and expressed as a percentage along the longitudinal axis of the spinal cord (Fig. 4*A*,*B*). We found that GAP-43 staining was significantly enhanced in both the rostral and caudal regions in K-II or C-ABC-treated rats compared with vehicle control rats (Fig. 4*B*). The raphespinal tract is partly responsible for motor function in rodents, and consists of serotonin (5-HT)-positive fibers. 5-HT staining showed a striking decrease in 5-HT-positive fibers in the rostral region, especially in vehicle control rats, but K-II and C-ABC significantly increased the number of stained fibers (Fig. 4*B*). On the other hand, in the caudal region, vehicle controls showed almost no stained fibers, whereas K-II and C-ABC significantly increased the number of stained fibers (Fig. 4*B*). Representative photos of GAP-45 and 5-HT staining around the lesion were presented in Figure 4*C*. These results are consistent with the idea that K-II or C-ABC significantly promoted axonal regrowth after SCI.

Furthermore, we performed anterograde labeling of CST to evaluate axonal growth and sprouting. In tracer fiber counts for the CST, we found many fibers stained in the region rostral to the epicenter (supplemental Fig. 3, available at www.jneurosci.org as supplemental material). There was no difference among the three groups in the rostral region (Fig. 4*D*). BDA-positive fibers were barely detectable in the caudal region of the vehicle group (Fig. 4*D*,*E*). These findings support the idea that this contusion model almost completely destroyed CST at the epicenter, and thus BDA-

←

(*Figure legend continued.*) axons 10 mm rostral to the lesioned site. No significant difference was observed between treatment groups. The bottom graph represents the ratio of labeled corticospinal axons 4 and 10 mm caudal versus 10 mm rostral to the lesioned site. K-II-treated rats had significantly more BDA-positive fibers at 4 and 10 mm caudal to the lesioned site than vehicle-treated rats. Data represent the means ± SEM. $*p < 0.05$; $**p < 0.005$ versus the vehicle control ($n = 7$ Vehicle; $n = 6$ C-ABC; $n = 5$ K-II). ***E***, Representative axial sections of the spinal cord taken from 10 mm caudal from the lesioned site at 10 weeks after SCI. The boxed areas are magnified on the right side of the panel. BDA-positive fibers were clearly seen in the section of K-II-treated rat (arrows). Scale bars, 500 μm for the left panel; 100 μm for the right panels. The thin silicone tube of an osmotic mini-pump (*) remained at a point 10 mm caudal from the epicenter. WM, White matter; GM, gray matter.

positive fibers hardly passed through the lesion to the caudal region in the vehicle group. In contrast, in K-II- and C-ABC-treated rats, the number of BDA-positive fibers was significantly increased in the region caudal to the epicenter, particularly in the gray matter in this region (Fig. 4*D*,*E*). These BDA-positive fibers in the gray matter may reflect growth or sprouting of proximal or spared axons.

Restoration of neurite outgrowth by K-II

Proteoglycans purified from the brains of chicks contain both KS and CS. We previously determined 300 ng/ml as the appropriate concentration of proteoglycans to coat dishes, which did not affect cell attachment but inhibited neurite outgrowth (Ito et al., 2010). Accordingly, the substratum coated with these proteoglycans strongly inhibited neurite outgrowth (Fig. 5*A*,*B*), whereas cell binding to the substratum was comparable between conditions tested (Fig. 5*A*). The proteoglycan-mediated inhibition of neurite growth was blocked by K-II and C-ABC, and the effects of K-II and C-ABC were comparable to each other, and also consistent with our previous study (Ito et al., 2010). To our surprise, the combination of K-II and C-ABC showed neither synergistic nor additive effects (Fig. 5*B*). Thus, these *in vitro* results were consistent with the *in vivo* phenomena. We also found that heat-denatured proteoglycans as well as reduced/alkylated proteoglycans lost their inhibitory activity (Fig. 5*C*), suggesting that the conformation of the core protein structure is also essential to this inhibition, since proteins rather than sugar chains are labile to heat or reduction/alkylation.

As K-II digests KS into oligosaccharides that are each composed of two to four saccharides, we addressed whether or not these degradation products of KS reversed the proteoglycan-mediated inhibition of neurite growth. However, KS-derived oligosaccharides (Fig. 5*D*) showed no promotion of neurite growth (Fig. 5*E*). These results exclude the possibility that the K-II-induced degradation products of KS promote neurite outgrowth, and suggest that K-II directly blocks the inhibition of neurite outgrowth by proteoglycans.

Neurite growth inhibition by KS/CSPG

Based on these *in vivo* and *in vitro* results, we hypothesized that K-II and C-ABC work on the same axis. We chose aggrecan as a model molecule, as it harbors both KS and CS chains (Fig. 6*A*) and is a representative proteoglycan in the CNS. Aggrecan strikingly inhibited axonal outgrowth

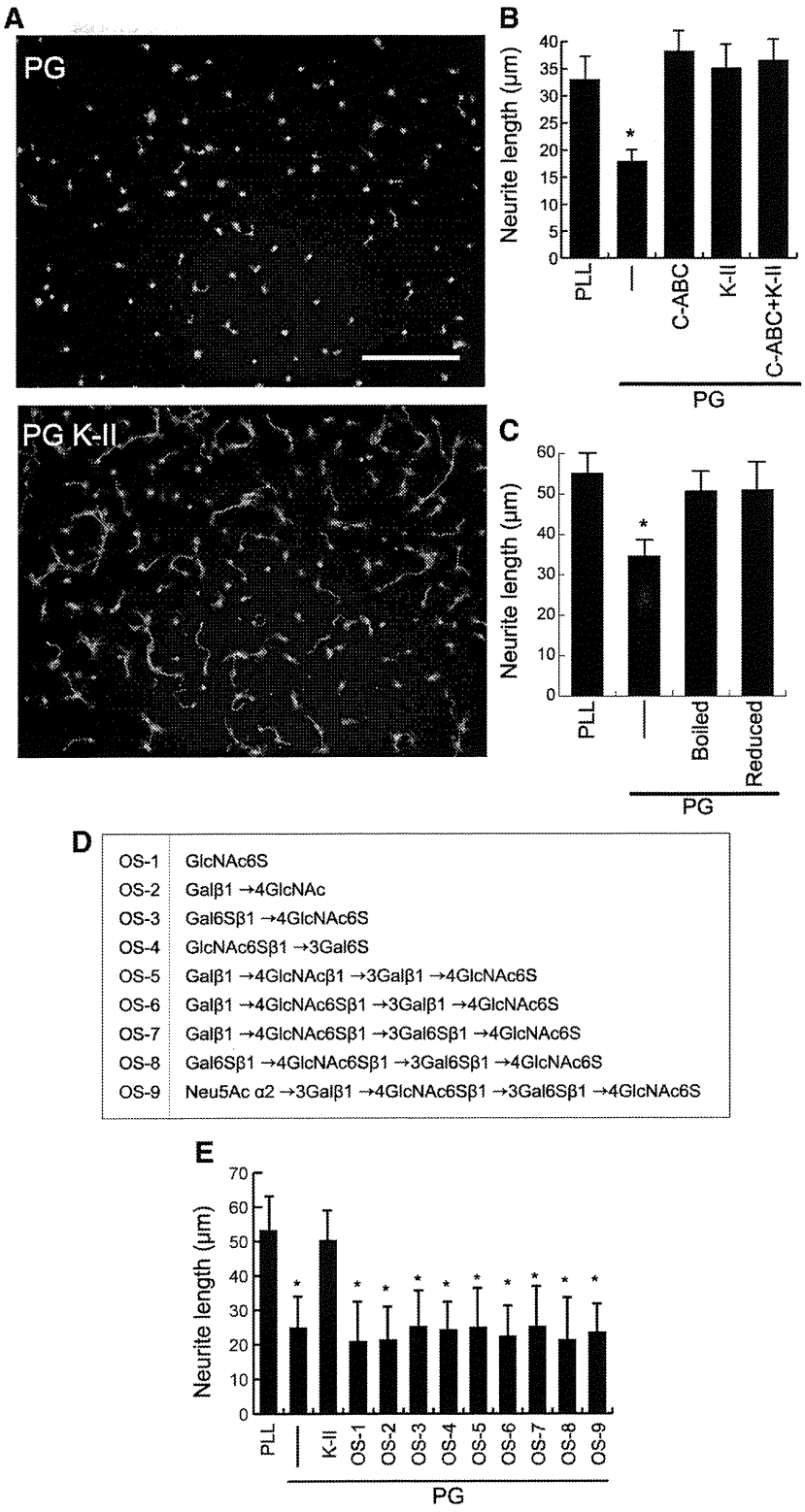

Figure 5. Restoration of neurite outgrowth by K-II. ***A***, P8 rat cerebellar granular neurons were cultured on proteoglycan (PG) extracted from chick brains. K-II treatment restored neurite outgrowth (PG K-II). Scale bar, 100 μm. ***B***, The quantification of ***A***. *$p < 0.05$ versus PLL. PG (300 ng/ml), C-ABC (200 mU/ml), and K-II (5 mU/ml) were used. Data represent the average neurite length ± SD. ***C***, Heat-denatured PG lost its neurite outgrowth-inhibitory activity. Data represent the average neurite length ± SD. *$p < 0.05$ versus PLL. ***D***, Structures of the oligosaccharides used in this experiment. ***E***, P8 rat cerebellar granular neurons were cultured on chick brain PG substrate in the absence or presence of oligosaccharides (1 μg/ml). Data represent the average neurite lengths ± SD. *$p < 0.05$ versus PLL.

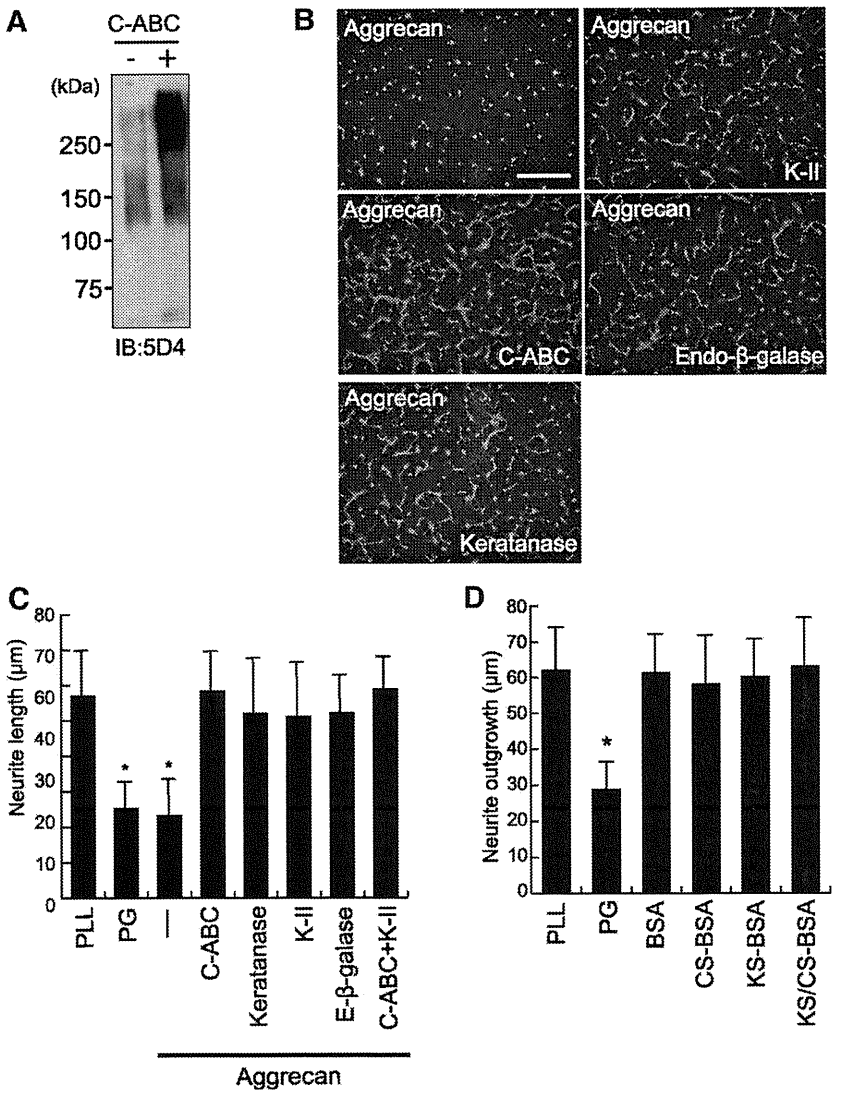

Figure 6. Effects of KS/CSPGs on neurite outgrowth. ***A***, Bovine aggrecan was digested with C-ABC (500 mU/ml) and subjected to SDS-PAGE using 5D4. Note that C-ABC treatment exposed KS epitopes. ***B***, P8 rat cerebellar granule neurons were cultured on aggrecan (5 μg/ml). Degradation of CS or KS restored neurite outgrowth. Scale bar, 100 μm. ***C***, The quantification of ***B***. Data represent the average neurite length ± SD. *$p < 0.05$ versus PLL. ***D***, There was no inhibition of neurite outgrowth by CS-BSA, KS-BSA, or KS/CS-BSA (300 ng/ml each). Data represent the average neurite length ± SD. *$p < 0.05$ versus PLL.

(Fig. 6*B*,*C*), consistent with previous studies (Asher et al., 1995; Johnson et al., 2002). The inhibition by aggrecan was as strong as that by a mixture of proteoglycans (Fig. 6*C*). Interestingly, this inhibition was reversed by C-ABC as well as K-II. Furthermore, the combination of these enzymes did not show additive or synergistic effects (Fig. 6*C*).

While K-II digested monosulfated and disulfated KS, keratanase digested monosulfated KS but not disulfated KS. The latter also reversed aggrecan-mediated inhibition of neurite outgrowth (Fig. 6*B*,*C*). Endo-β-galactosidase, which digests KS and polylactosamine, provided the same effect (Fig. 6*B*,*C*). These results collectively indicate that KS of aggrecan is required for the aggrecan-mediated inhibition of neurite outgrowth.

We then generated an artificial proteoglycan consisting of BSA, KS, and CS. In this experiment, we tried to understand how the three components of KS/CSPG (core protein, CS chains, and KS chains) are needed to exert the inhibitory activity. The estimated ratios of the core protein (BSA), CS, and KS in KS/CS-BSA were 1:30:84. Because the ratio in human aggrecan is 1:100:60 (Kiani et al., 2002), KS/CS-BSA was considered suitable for examining the function of KS, CS, and the core protein. However, KS/CS-BSA failed to inhibit neurite outgrowth (Fig. 6*D*). KS-BSA and CS-BSA also failed to do so (Fig. 6*D*).

Discussion

So far, KSPGs and CSPGs have been studied independently, and KSPGs have not been extensively studied. Our study has integrated KS and CS into a common axis. K-II and C-ABC strikingly promoted functional recovery after SCI. GAP-43, 5-HT staining, and CST tracer fiber count were significantly enhanced in K-II- or C-ABC-treated rats compared with vehicle control rats. Although the striking functional recovery may not be necessarily consistent with the data from the histological analyses, this may have been partly due to the limited ability to detect outgrowing axons by the antibodies and the tracer compound used. We found that the effects of K-II and C-ABC on *in vivo* functional disturbance after SCI and *in vitro* neurite outgrowth inhibition mediated by proteoglycans were comparable to each other. However, both *in vivo* and *in vitro*, the combination of these two enzymes showed neither additive nor synergistic effects. It should be noted that the peptide linkage region for CS always consists of xylose, galactose, and glucuronic acid, whereas the KS chain is elongated from ordinary *N*-linked or *O*-linked sugar chains. Thus, each glycosaminoglycan exists as an independent sugar chain. For example, human aggrecan is composed of a core protein and CS and KS chains at a ratio of 1:100:60 (Kiani et al., 2002). Together, our study has established that KS and CS are independently required for the inhibition of postinjury neural plasticity and neurite outgrowth.

Furthermore, we found that neurite outgrowth was not inhibited by heat-denatured proteoglycans or by reduced/alkylated proteoglycans. This inhibition was also not achieved by an artificial KS/CSPG, KS/CS-albumin, whereas the natural KS/CSPG aggrecan inhibited neurite outgrowth. Our results thus far obtained are summarized in Figure 7*A*. Our data suggest that the three components (KS, CS, and core protein) of the proteoglycan moiety are interdependent and required for proteoglycan-mediated inhibition of structural rearrangement after neuronal injuries.

It is important to point out that there is a much smaller amount of KS than CS in the CNS, and our data supported this idea (Fig. 1*B*,*C*). The family of KSPGs is also smaller than that of CSPGs (Margolis and Margolis, 1993; Funderburgh, 2000, 2002). In this context, it was surprising to us that K-II shows activity

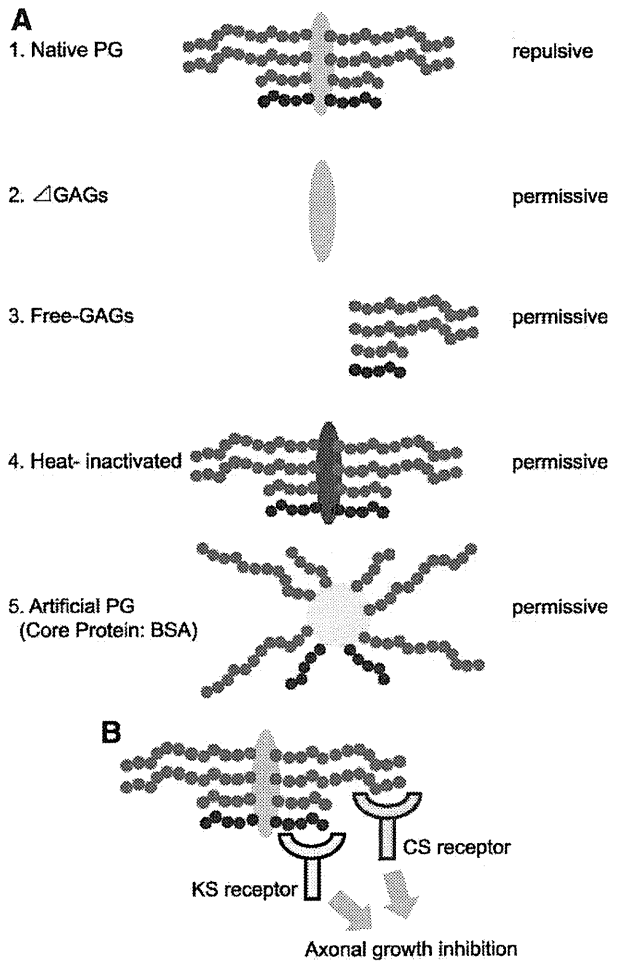

Figure 7. Structure and function relationship in the proteoglycan (PG)-mediated inhibition of neurite growth. ***A***, The present study has revealed that KS and CS have a comparable impact on PG-mediated inhibition of neurite growth. Considering our previous results that neither KS nor CS is sufficient for neurite growth inhibition (Ito et al., 2010), our data suggest that all three components of the proteoglycans moiety (core protein, CS, and KS) are required for this inhibition activity. ***B***, This scheme shows a speculated mechanism underlying the PG-mediated inhibition of axonal growth.

comparable to that of C-ABC *in vivo* and *in vitro*. Although further investigations are needed, we speculate the following mechanism (summarized in Fig. 7*B*), based on our observations. First, although KS is composed of repeating disaccharide units, the composition is heterogeneous, i.e., there are highly sulfated disaccharide clusters as well as poorly sulfated disaccharide clusters in a KS chain. Therefore, it is conceivable that there is a functional domain in a KS chain (e.g., a highly sulfated stretch of 6–8 saccharides). This is also the case in a CS chain (there are 4 different sulfation variations in CS—CS-A, -C, -D, and -E units). Second, these functional domains may appear more frequently in KS than in CS. Finally, these functional domains may be recognized independently by specific receptors so that KS and CS are independently required for the inhibition of neurite outgrowth (Fig. 7*B*). Our idea is partly supported by the recent report that PTPσ is the receptor for CS (Shen et al., 2009; Coles et al., 2011). However, there is another possibility. C-ABC might not be very stable, although a significant portion of CS appeared to be lost by C-ABC treatment on Western blot analysis (Fig. 1*C*). Thus, we should not exclude the possibility that an insufficient *in vivo* digestion of CS by our current method led to the lack of synergism of K-II and C-ABC.

Reported data regarding the biological impacts of KS and CS on neurite outgrowth have been contradictory. For example, Powell et al. (1997) reported *in vitro* data that showed the effects of CS and KS are similar, but that enzymatic treatment with C-ABC and keratanase is synergistic. In contrast, Snow et al. (1990b) showed that *in vitro* enzymatic removal of KS and CS from CSPGs differ with regard to neurite behavior (CS is stronger than KS). Furthermore, in cultured hippocampal slices, keratanase, but not C-ABC, leads to misrouting of mossy fibers (Butler et al., 2004). In the present study, we conducted experiments both *in vivo* and *in vitro* to address the same issue. Our study has revealed that KS and CS are independent requirements for the proteoglycan-mediated inhibition of postinjury neural plasticity *in vivo*. Taking into account that the K-II used for *in vivo* experiments in the present study is relatively stable at 37°C and has a wide window of therapeutic doses, our *in vivo* data may be reliable. *In vitro* results were consistent with *in vivo* data. Although discrepancy between reports might be due to different conditions examined, our results may provide a hint for further studies on molecular mechanisms of the neural plasticity regulation by proteoglycans.

The functional recovery by K-II or C-ABC after SCI may not simply rely on neurite outgrowth promotion by these enzymes. The ECM surrounding neurons forms a lace-like structure, the so-called perineuronal net (Takahashi-Iwanaga et al., 1998), and is essentially composed of hyaluronic acid and proteoglycans. Perineuronal nets are prominent on GABAergic interneurons, but can be detected on virtually all neurons (Celio and Blümcke, 1994; Celio et al., 1998; John et al., 2006). This ECM may inhibit structural rearrangements at synapses, thereby contributing to the maintenance of neuronal networks; this idea is supported by recent works showing that C-ABC promotes synaptic plasticity and dendritic spine dynamics (Pizzorusso et al., 2002, 2006; Berardi et al., 2004; Oray et al., 2004). C-ABC restores the plasticity of not only sensory networks but also emotional networks (Pizzorusso et al., 2002; Gogolla et al., 2009). Furthermore, hyaluronidase, a hyaluronic acid-degrading enzyme, and C-ABC increase AMPA receptor lateral mobility, and consequently modulate short-term synaptic plasticity (Frischknecht et al., 2009). Considering these data together, our results suggest that K-II and C-ABC may remove the ECM and promote structural rearrangement of neuronal networks after SCI. In this context, it is an interesting challenge to ask whether K-II also restores ocular dominance plasticity in adults.

Regarding the lateral mobility of membrane molecules such as AMPA receptor on dendrites, the ECM works as a viscous diffusion constraint that slows and confines the mobility of molecules entering the ECM-covered compartments (Frischknecht et al., 2009). Thus, a general function of the ECM is to act as a passive barrier. On the other hand, it has recently been reported that PTPσ acts as a receptor for CS and mediates the inhibitory activity of CSPGs on axonal regeneration (Shen et al., 2009). Our data raise the intriguing possibility that a KS-specific receptor may also exist (Fig. 7*B*).

It is also important to consider that KS degradation within the intact area may cause maladaptive plasticity if K-II affects the ECM structure. However, as shown in Figure 3, K-II administration promoted recovery from thermal hyperalgesia and mechanical allodynia. Thus, the delivery method used in our study could minimize the unwanted adverse effect of KS degradation. Supporting this idea, we observed that *in vivo* KS degradation by K-II

was good enough to promote functional recovery, but not completely abolish KS, probably due to a limited diffusion of infused enzyme.

In addition to the therapeutic effects of K-II on SCI, we also noticed that the functional recovery induced by K-II or C-ABC was not complete. Therefore, further improvement of a therapeutic strategy for SCI must be considered. García-Alías et al. (2009) recently reported that a combination of C-ABC and rehabilitation leads to a striking functional recovery after SCI at the cervical level. Even if our present results suggest that K-II or C-ABC may promote not only axonal regrowth but also neural plasticity related to motor and sensory function, other efforts, such as rehabilitation, to improve the reestablishment of neural circuitry would be helpful to realize a satisfactory treatment for SCI.

References

Asher RA, Scheibe RJ, Keiser HD, Bignami A (1995) On the existence of a cartilage-like proteoglycan and link proteins in the central nervous system. Glia 13:294–308.

Basso DM, Beattie MS, Bresnahan JC (1995) A sensitive and reliable locomotor rating scale for open field testing in rats. J Neurotrauma 12:1–21.

Berardi N, Pizzorusso T, Maffei L (2004) Extracellular matrix and visual cortical plasticity: freeing the synapse. Neuron 44:905–908.

Bradbury EJ, Moon LD, Popat RJ, King VR, Bennett GS, Patel PN, Fawcett JW, McMahon SB (2002) Chondroitinase ABC promotes functional recovery after spinal cord injury. Nature 416:636–640.

Butler CD, Schnetz SA, Yu EY, Davis JB, Temple K, Silver J, Malouf AT (2004) Keratan sulfate proteoglycan phosphacan regulates mossy fiber outgrowth and regeneration. J Neurosci 24:462–473.

Celio MR, Blümcke I (1994) Perineuronal nets—a specialized form of extracellular matrix in the adult nervous system. Brain Res Brain Res Rev 19:128–145.

Celio MR, Spreafico R, De Biasi S, Vitellaro-Zuccarello L (1998) Perineuronal nets: past and present. Trends Neurosci 21:510–515.

Cole GJ, McCabe CF (1991) Identification of a developmentally regulated keratan sulfate proteoglycan that inhibits cell adhesion and neurite outgrowth. Neuron 7:1007–1018.

Coles CH, Shen Y, Tenney AP, Siebold C, Sutton GC, Lu W, Gallagher JT, Jones EY, Flanagan JG, Aricescu AR (2011) Proteoglycan-specific molecular switch for RPTPσ clustering and neuronal extension. Science 332:484–488.

Davies SJ, Goucher DR, Doller C, Silver J (1999) Robust regeneration of adult sensory axons in degenerating white matter of the adult rat spinal cord. J Neurosci 19:5810–5822.

Frischknecht R, Heine M, Perrais D, Seidenbecher CI, Choquet D, Gundelfinger ED (2009) Brain extracellular matrix affects AMPA receptor lateral mobility and short-term synaptic plasticity. Nat Neurosci 12:897–904.

Funderburgh JL (2000) Keratan sulfate: structure, biosynthesis, and function. Glycobiology 10:951–958.

Funderburgh JL (2002) Keratan sulfate biosynthesis. IUBMB Life 54:187–194.

García-Alías G, Barkhuysen S, Buckle M, Fawcett JW (2009) Chondroitinase ABC treatment opens a window of opportunity for task-specific rehabilitation. Nat Neurosci 12:1145–1151.

Geisert EE Jr, Bidanset DJ, Del Mar N, Robson JA (1996) Up-regulation of a keratan sulfate proteoglycan following cortical injury in neonatal rats. Int J Dev Neurosci 14:257–267.

Gogolla N, Caroni P, Lüthi A, Herry C (2009) Perineuronal nets protect fear memories from erasure. Science 325:1258–1261.

Grimpe B, Silver J (2004) A novel DNA enzyme reduces glycosaminoglycan chains in the glial scar and allows microtransplanted dorsal root ganglia axons to regenerate beyond lesions in the spinal cord. J Neurosci 24:1393–1397.

Hutchinson KJ, Gómez-Pinilla F, Crowe MJ, Ying Z, Basso DM (2004) Three exercise paradigms differentially improve sensory recovery after spinal cord contusion in rats. Brain 127:1403–1414.

Ito Z, Sakamoto K, Imagama S, Matsuyama Y, Zhang H, Hirano K, Ando K, Yamashita T, Ishiguro N, Kadomatsu K (2010) *N*-acetylglucosamine 6-*O*-sulfotransferase-1-deficient mice show better functional recovery after spinal cord injury. J Neurosci 30:5937–5947.

John N, Krügel H, Frischknecht R, Smalla KH, Schultz C, Kreutz MR, Gundelfinger ED, Seidenbecher CI (2006) Brevican-containing perineuronal nets of extracellular matrix in dissociated hippocampal primary cultures. Mol Cell Neurosci 31:774–784.

Johnson WE, Caterson B, Eisenstein SM, Hynds DL, Snow DM, Roberts S (2002) Human intervertebral disc aggrecan inhibits nerve growth in vitro. Arthritis Rheum 46:2658–2664.

Jones LL, Tuszynski MH (2002) Spinal cord injury elicits expression of keratan sulfate proteoglycans by macrophages, reactive microglia, and oligodendrocyte progenitors. J Neurosci 22:4611–4624.

Kiani C, Chen L, Wu YJ, Yee AJ, Yang BB (2002) Structure and function of aggrecan. Cell Res 12:19–32.

Krautstrunk M, Scholtes F, Martin D, Schoenen J, Schmitt AB, Plate D, Nacimiento W, Noth J, Brook GA (2002) Increased expression of the putative axon growth-repulsive extracellular matrix molecule, keratan sulphate proteoglycan, following traumatic injury of the adult rat spinal cord. Acta Neuropathol 104:592–600.

Margolis RK, Margolis RU (1993) Nervous tissue proteoglycans. Experientia 49:429–446.

Massey JM, Hubscher CH, Wagoner MR, Decker JA, Amps J, Silver J, Onifer SM (2006) Chondroitinase ABC digestion of the perineuronal net promotes functional collateral sprouting in the cuneate nucleus after cervical spinal cord injury. J Neurosci 26:4406–4414.

Moon LD, Asher RA, Rhodes KE, Fawcett JW (2001) Regeneration of CNS axons back to their target following treatment of adult rat brain with chondroitinase ABC. Nat Neurosci 4:465–466.

Moon LD, Asher RA, Rhodes KE, Fawcett JW (2002) Relationship between sprouting axons, proteoglycans and glial cells following unilateral nigrostriatal axotomy in the adult rat. Neuroscience 109:101–117.

Oray S, Majewska A, Sur M (2004) Dendritic spine dynamics are regulated by monocular deprivation and extracellular matrix degradation. Neuron 44:1021–1030.

Pizzorusso T, Medini P, Berardi N, Chierzi S, Fawcett JW, Maffei L (2002) Reactivation of ocular dominance plasticity in the adult visual cortex. Science 298:1248–1251.

Pizzorusso T, Medini P, Landi S, Baldini S, Berardi N, Maffei L (2006) Structural and functional recovery from early monocular deprivation in adult rats. Proc Natl Acad Sci U S A 103:8517–8522.

Powell EM, Fawcett JW, Geller HM (1997) Proteoglycans provide neurite guidance at an astrocyte boundary. Mol Cell Neurosci 10:27–42.

Properzi F, Carulli D, Asher RA, Muir E, Camargo LM, van Kuppevelt TH, ten Dam GB, Furukawa Y, Mikami T, Sugahara K, Toida T, Geller HM, Fawcett JW (2005) Chondroitin 6-sulphate synthesis is up-regulated in injured CNS, induced by injury-related cytokines and enhanced in axon-growth inhibitory glia. Eur J Neurosci 21:378–390.

Pumphrey CY, Theus AM, Li S, Parrish RS, Sanderson RD (2002) Neoglycans, carbodiimide-modified glycosaminoglycans: a new class of anticancer agents that inhibit cancer cell proliferation and induce apoptosis. Cancer Res 62:3722–3728.

Rapalino O, Lazarov-Spiegler O, Agranov E, Velan GJ, Yoles E, Fraidakis M, Solomon A, Gepstein R, Katz A, Belkin M, Hadani M, Schwartz M (1998) Implantation of stimulated homologous macrophages results in partial recovery of paraplegic rats. Nat Med 4:814–821.

Shen Y, Tenney AP, Busch SA, Horn KP, Cuascut FX, Liu K, He Z, Silver J, Flanagan JG (2009) PTPσ is a receptor for chondroitin sulfate proteoglycan, an inhibitor of neural regeneration. Science 326:592–596.

Shinmei M, Miyauchi S, Machida A, Miyazaki K (1992) Quantitation of chondroitin 4-sulfate and chondroitin 6-sulfate in pathologic joint fluid. Arthritis Rheum 35:1304–1308.

Silver J, Miller JH (2004) Regeneration beyond the glial scar. Nat Rev Neurosci 5:146–156.

Sivasankaran R, Pei J, Wang KC, Zhang YP, Shields CB, Xu XM, He Z (2004) PKC mediates inhibitory effects of myelin and chondroitin sulfate proteoglycans on axonal regeneration. Nat Neurosci 7:261–268.

Snow DM, Steindler DA, Silver J (1990a) Molecular and cellular characterization of the glial roof plate of the spinal cord and optic tectum: a possible role for a proteoglycan in the development of an axon barrier. Dev Biol 138:359–376.

Snow DM, Lemmon V, Carrino DA, Caplan AI, Silver J (1990b) Sulfated

proteoglycans in astroglial barriers inhibit neurite outgrowth *in vitro*. Exp Neurol 109:111–130.

Sutter M, Deletis V, Dvorak J, Eggspuehler A, Grob D, Macdonald D, Mueller A, Sala F, Tamaki T (2007) Current opinions and recommendations on multimodal intraoperative monitoring during spine surgeries. Eur Spine J 16 [Suppl 2]:S232–S237.

Takahashi-Iwanaga H, Murakami T, Abe K (1998) Three-dimensional microanatomy of perineuronal proteoglycan nets enveloping motor neurons in the rat spinal cord. J Neurocytol 27:817–827.

Tamaki T, Kubota S (2007) History of the development of intraoperative spinal cord monitoring. Eur Spine J 16 [Suppl 2]:S140–S146.

Tom VJ, Steinmetz MP, Miller JH, Doller CM, Silver J (2004) Studies on the development and behavior of the dystrophic growth cone, the hallmark of regeneration failure, in an *in vitro* model of the glial scar and after spinal cord injury. J Neurosci 24:6531–6539.

Yamagishi K, Suzuki K, Imai K, Mochizuki H, Morikawa K, Kyogashima M, Kimata K, Watanabe H (2003) Purification, characterization, and molecular cloning of a novel keratan sulfate hydrolase, endo-β-*N*-acetylglucosaminidase, from *Bacillus circulans*. J Biol Chem 278: 25766–25772.

Zhang H, Muramatsu T, Murase A, Yuasa S, Uchimura K, Kadomatsu K (2006) *N*-Acetylglucosamine 6-*O*-sulfotransferase-1 is required for brain keratan sulfate biosynthesis and glial scar formation after brain injury. Glycobiology 16:702–710.

Research article

Human dental pulp-derived stem cells promote locomotor recovery after complete transection of the rat spinal cord by multiple neuro-regenerative mechanisms

Kiyoshi Sakai,[1] Akihito Yamamoto,[1] Kohki Matsubara,[1] Shoko Nakamura,[1] Mami Naruse,[1] Mari Yamagata,[1] Kazuma Sakamoto,[2] Ryoji Tauchi,[3] Norimitsu Wakao,[3] Shiro Imagama,[3] Hideharu Hibi,[1] Kenji Kadomatsu,[2] Naoki Ishiguro,[3] and Minoru Ueda[1]

[1]Department of Oral and Maxillofacial Surgery, [2]Department of Biochemistry, and [3]Department of Orthopedic Surgery, Nagoya University Graduate School of Medicine, Nagoya, Japan.

Spinal cord injury (SCI) often leads to persistent functional deficits due to loss of neurons and glia and to limited axonal regeneration after injury. Here we report that transplantation of human dental pulp stem cells into the completely transected adult rat spinal cord resulted in marked recovery of hind limb locomotor functions. Transplantation of human bone marrow stromal cells or skin-derived fibroblasts led to substantially less recovery of locomotor function. The human dental pulp stem cells exhibited three major neuroregenerative activities. First, they inhibited the SCI-induced apoptosis of neurons, astrocytes, and oligodendrocytes, which improved the preservation of neuronal filaments and myelin sheaths. Second, they promoted the regeneration of transected axons by directly inhibiting multiple axon growth inhibitors, including chondroitin sulfate proteoglycan and myelin-associated glycoprotein, via paracrine mechanisms. Last, they replaced lost cells by differentiating into mature oligodendrocytes under the extreme conditions of SCI. Our data demonstrate that tooth-derived stem cells may provide therapeutic benefits for treating SCI through both cell-autonomous and paracrine neuroregenerative activities.

Introduction

The development of effective treatments for spinal cord injury (SCI) has been stifled by this injury's complicated pathophysiology (1). During the acute phase, the focal mechanical insult disrupts tissue homeostasis. This triggers secondary injury processes in which multiple destructive cascades cause the necrotic and apoptotic death of neurons, astrocytes, and oligodendrocytes, which spreads beyond the initial injury site and leads to irreversible axonal damage and demyelination (2, 3). Subsequently, reactive astrocytes and oligodendrocytes near the site of injured spinal cord (SC) respectively produce chondroitin sulfate proteoglycans (CSPGs) and myelin proteins (including myelin-associated glycoprotein [MAG], Nogo, oligodendrocyte myelin glycoprotein [OMgp], netrin, semaphorin, and ephrin). These extracellular molecules function as axon growth inhibitors (AGIs), acting through the intracellular Rho GTPase signaling cascade (4). These multiple pathogenic signals synergistically accelerate the progressive deterioration after SCI. Therefore, therapeutic strategies for functional recovery from SCI must exert multifaceted reparative effects against a variety of pathogeneses (2).

Stem cell–based transplantation therapy holds great promise for establishing such a multifaceted therapeutic strategy. In the last decade, a variety of cell types, including human neural stem cells (5), embryonic stem cell derivatives (6–8), and adult bone marrow stromal cells (BMSCs) (9, 10), have been transplanted into the injured SC of rats or mice, and their neuroregenerative activities evaluated. These preclinical studies showed that engrafted stem cells promote substantial functional recovery after SCI through both cell-autonomous/cell-replacement and paracrine/trophic effects (11). However, the previously tested stem cells show poor survival (6–8, 12) and/or differentiation under the severe conditions of SCI (9, 13, 14), and the transplantation of individual stem cells has led to only modest therapeutic benefits. Furthermore, although the trophic factors derived from these stem cells promote in vitro neurite extension and survival, their roles in the functional recovery of SCI are still largely unknown.

Human adult dental pulp stem cells (DPSCs) and stem cells from human exfoliated deciduous teeth (SHEDs) are self-renewing stem cells residing within the perivascular niche of the dental pulp (15). They are thought to originate from the cranial neural crest and express early markers for both mesenchymal and neuroectodermal stem cells (16, 17). Since naturally exfoliated deciduous and impacted adult wisdom teeth are not usually needed, DPSCs and SHEDs can be obtained without adverse health effects. Similar to BMSCs, these cells are able to differentiate into osteoblasts, chondrocytes, adipocytes, endothelial cells, and functionally active neurons in vitro, under defined conditions (16–19). Trophic factors expressed by them promote neuronal survival, proliferation, differentiation, and migration (20–23). Thus, these previous reports support the use of tooth-derived stem cells as a unique cellular resource for neuroregeneration therapies. However, their ability to promote functional recovery in neurological disorders remains largely unknown.

Authorship note: Kiyoshi Sakai and Akihito Yamamoto contributed equally to this work.

Conflict of interest: The authors have declared that no conflict of interest exists.

Citation for this article: *J Clin Invest.* 2012;122(1):80–90. doi:10.1172/JCI59251.

Table 1
Flow cytometry of stem cells from humans

	SHEDs ($n = 3$)		DPSCs ($n = 3$)		BMSCs ($n = 3$)	
	Positive (%)	SD	Positive (%)	SD	Positive (%)	SD
MSC markers						
CD90	98.25	0.91	98.96	0.95	≥90	
CD73	91.45	8.44	96.60	2.14	≥90	
CD105	98.20	2.44	98.23	0.54	≥90	
Negative markers						
CD45	0.33	0.28	0.11	0.09	≤10	
CD34	0.36	0.32	0.07	0.03	≤10	
CD11b	0.02	0.02	0.03	0.02	≤10	
HLA-DR	0.45	0.39	0.12	0.10	≤10	
Neural markers						
DCX	95.42	0.66	84.45	0.45	91.37	8.20
Nestin	92.71	10.46	95.40	1.52	35.76	8.06
GFAP	92.93	8.30	97.50	3.54	4.49	3.11
βIII-Tubulin	99.69	0.21	85.43	0.77	99.24	0.73
NeuN	31.93	7.25	26.61	4.28	2.97	1.74
A2B5	94.84	3.72	96.34	0.33	35.47	15.07
CNPase	99.21	0.11	98.19	0.46	21.35	7.81
APC	0.20	0.01	0.36	0.02	2.75	2.05
MBP	0.68	0.04	0.32	0.02	3.02	2.00

Here we examined the neuroregenerative activities of DPSCs and SHEDs by transplanting them into a completely transected rat SCI model during the acute phase, in which axonal regeneration rather than axonal sprouting can be evaluated accurately. Our data show that these tooth-derived stem cells promoted functional recovery after SCI by multifaceted neuro-regenerative activities, via both cell-autonomous/cell replacement and paracrine/trophic mechanisms.

Results

Characterization of isolated human SHEDs and DPSCs for use in transplantation studies. Flow cytometry analysis showed that the SHEDs and DPSCs expressed a set of mesenchymal stem cell (MSC) markers (i.e., CD90, CD73, and CD105), but not endothelial/hematopoietic markers (i.e., CD34, CD45, CD11b/c, and HLA-DR) (Table 1). Like human BMSCs, both the SHEDs and DPSCs exhibited adipogenic, chondrogenic, and osteogenic differentiation as described previously (refs. 16, 17, and data not shown). The majority of SHEDs and DPSCs coexpressed several neural lineage markers: nestin (neural stem cells), doublecortin (DCX; neuronal progenitor cells), βIII-tubulin (early neuronal cells), NeuN (mature neurons), GFAP (neural stem cells and astrocytes), S-100 (Schwann cells), and A2B5 and CNPase (oligodendrocyte progenitor cells), but not adenomatous polyposis coli (APC) or myelin basic protein (MBP) (mature oligodendrocytes) (Figure 1A and Table 1). This expression profile was confirmed by immunohistochemical analyses (Figure 1B).

Next, we examined the expression of representative neurotrophic factors by real-time PCR. Both the SHEDs and DPSCs expressed glial cell–derived neurotrophic factor (*GDNF*), brain-derived neurotrophic factor (*BDNF*), and ciliary neurotrophic factor (*CNTF*) at more than 3 to 5 times the levels expressed by skin-derived fibroblasts or BMSCs (Figure 1C).

We further characterized the transcriptomes of SHEDs and BMSCs by cDNA microarray analysis. This gene expression analysis revealed a 2.0-fold difference in the expression of 3,318 of 41,078 genes between SHEDs and BMSCs. Of these, 1,718 genes were expressed at higher levels in the SHEDs and 1,593 genes were expressed at lower levels (data not shown). The top 30 genes showing higher expression in the SHEDs were in the following ontology categories: extracellular and cell surface region, cell proliferation, and tissue/embryonic development (Table 2).

SHEDs and DPSCs promoted locomotor recovery after SCI. To compare the neuroregenerative activities of human SHEDs and DPSCs with those of human BMSCs and human skin fibroblasts, we transplanted the cells into the completely transected SCs, as described in Methods, and evaluated locomotion recovery using the Basso, Beattie, Bresnahan locomotor rating scale (BBB scale) (24). Remarkably, the animals that received SHEDs or DPSCs exhibited a significantly higher BBB score during the entire observation period, compared with BMSC-transplanted, fibroblast-transplanted, or PBS-injected control rats (Figure 2A). Importantly, their superior recoveries were evident soon after the operation, during the acute phase of SCI. After the recovery period (5 weeks after the operation), the rats that had received SHEDs were able to move 3 joints of hind limb coordinately and walk without weight support ($P < 0.01$; Supplemental Videos 1 and 2), while the BMSC- or fibroblast-transplanted rats exhibited only subtle movements of 1–2 joints. These results demonstrate that the transplantation of SHEDs or DPSCs during the acute phase of SCI significantly improved the recovery of hind limb locomotor function. Since the level of recovery was similar in the SHED- and DPSC-transplanted rats, we focused on the phenotypical examination of SHED-transplanted rats to elucidate how tooth-derived stem cells promoted the regeneration of the completely transected rat SC.

SHEDs regenerated the transected corticospinal tract and raphespinal serotonergic axons. To examine whether engrafted SHEDs affect the preservation of neurofilaments, we performed immunohistochemical analyses with an anti–neurofilament M (NF-M) mAb, 8 weeks after transection. Compared with the PBS-treated control SCs, the SHED-transplanted SCs exhibited greater preservation of NF-positive axons from 3 mm rostral to 3 mm caudal to the transected lesion site (Figure 2, B and C; asterisk indicates epicenter). The percentages of NF-positive axons in the epicenter of the SHED-transplanted and control SCs were 35.8% ± 13.0% and 8.7% ± 3.4%, respectively, relative to sham-treated SCs (Figure 2D).

Regeneration of both the corticospinal tract (CST) and the descending serotonergic raphespinal axons is important for the recovery of hind limb locomotor function in rat SCI. We therefore examined whether these axons had extended beyond the epicenter in the SHED-transplanted SCs. The CST axons were traced with the anterograde tracer biotinylated dextran amine (BDA), which was injected into the sensorimotor cortex. The serotoner-

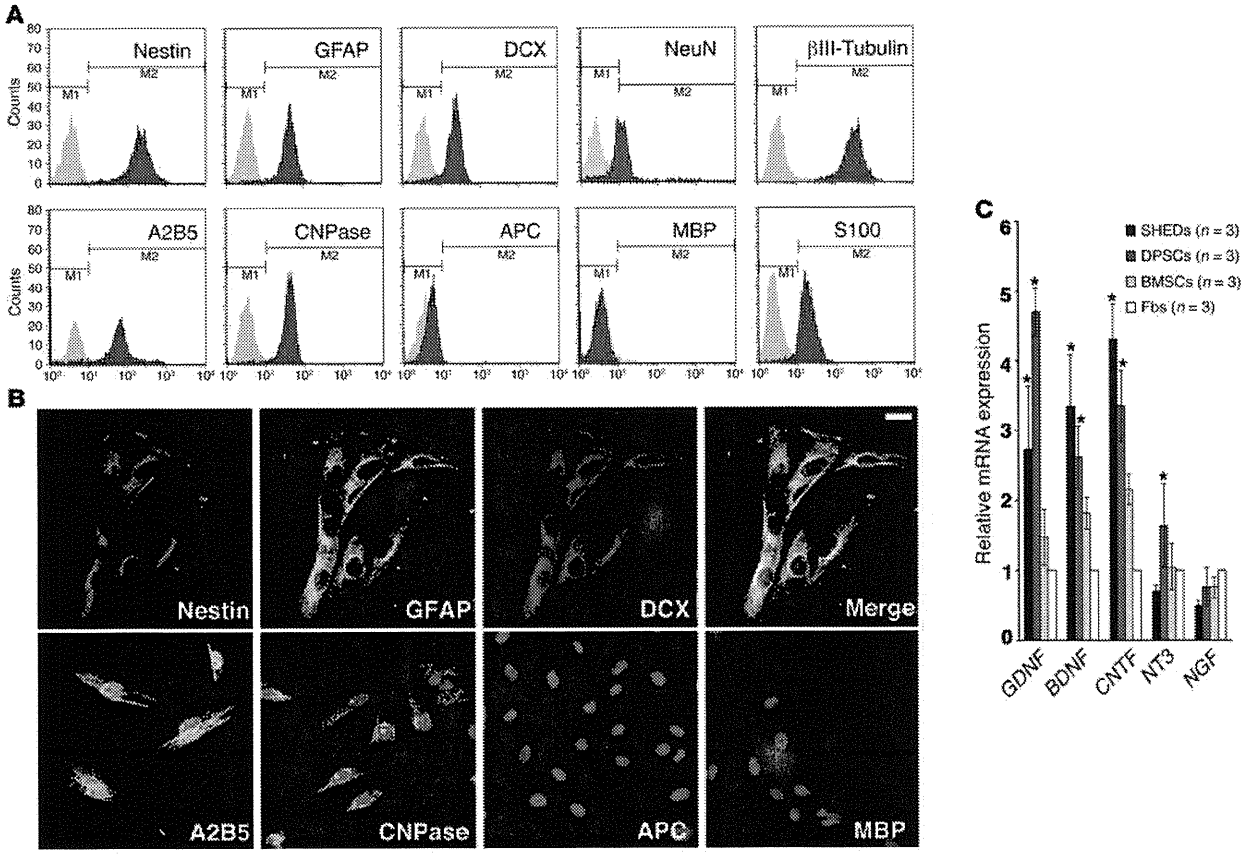

Figure 1

Characterization of the SHEDs and DPSCs used for transplantation. (**A**) Flow cytometry analysis of the neural cell lineage markers expressed in SHEDs. Note that most of the SHEDs and DPSCs coexpressed neural stem and multiple progenitor markers, but not mature oligodendrocytes (APC and MBP). (**B**) Confocal images showing SHEDs coexpressed nestin, GFAP, and DCX. SHEDs also expressed markers for oligodendrocyte progenitor cells (A2B5 and CNPase), but not for mature oligodendrocytes (APC and MBP). Scale bar: 10 μm. (**C**) Real-time RT-PCR analysis of the expression of neurotrophic factors. Results are expressed as fold increase compared with the level expressed in skin fibroblasts. Data represent the average measurements for each cell type from 3 independent donors. This set of experiments was repeated twice and yielded similar results. Data represent the mean ± SEM. $^*P < 0.01$ compared with BMSCs and fibroblasts (Fbs).

gic raphespinal axons were immunohistochemically detected by a mAb that specifically reacts with serotonin (5-hydroxytryptamine [5-HT]), which is synthesized within the brain stem. We found that both BDA- and 5-HT–positive fibers extended as far as 3 mm caudal to the epicenter in the SHED-transplanted but not the control group (Figures 3 and 4). Furthermore, some BDA- and 5-HT–positive boutons could be seen apposed to neurons in the caudal stump (Figure 3D and Figure 4C), suggesting that the regenerated axons had established new neural connections. Notably, although the number of descending axons extending beyond the epicenter was small, we observed many of them penetrating the scar tissue of the rostral stump (Figure 3A and Figure 4A). The percentages of 5-HT–positive axons of the SHED-transplanted SCs at 1 and 3 mm rostral to the epicenter were 58.9% ± 3.9% and 78.3% ± 7.4% relative to sham-treated SC, respectively (Figure 4D). These results demonstrate that the engrafted SHEDs promoted the recovery of hind limb locomotion via the preservation and regeneration of transected axons, even in the microenvironment of the damaged CNS.

SHEDs inhibited the Rho GTPase activity induced by SC transection. The apparent axon regeneration in the SHED-transplanted SCs suggested that the SHEDs might modulate multiple AGI signals generated from oligodendrocytes and reactive astrocytes forming the glial scar. We therefore measured the activity level of Rho GTPase, which is an intracellular target of multiple AGIs, by pull-down assay. The injured SCs were isolated 7 days after transection and subjected to immunoprecipitation with GST-tagged Rho-binding domain (RBD). The level of active Rho (GTP-bound Rho [GTP-Rho]) in the transected control SCs increased; however, the engrafted SHEDs remarkably inhibited the activation of Rho (Figure 4E). These results strongly suggest that SHEDs promoted axon regeneration through the inhibition of multiple AGI signals.

Serum-free conditioned medium from both SHEDs and DPSCs antagonizes CSPG- or MAG-mediated neurite growth inhibition. Next, to analyze the roles of trophic mechanisms in the SHED-mediated axon regeneration, we examined whether the conditioned medium (CM) from SHEDs (SHED-CM) or DPSCs (DPSC-CM) could promote the neurite extension of cerebral granular neurons (CGNs)

Table 2
Functional gene classification in SHEDs versus BMSCs

Term	Changed gene up	Total gene	P
Extracellular region	343	2,865	2.52×10^{-14}
Skeletal system development	104	661	1.46×10^{-9}
Extracellular matrix	101	678	9.20×10^{-9}
Extracellular space	147	1,134	2.00×10^{-8}
Extracellular matrix organization	43	195	4.86×10^{-8}
Multicellular organismal development	643	6,683	9.36×10^{-8}
Collagen fibril organization	20	57	4.97×10^{-7}
Anatomical structure morphogenesis	346	3,339	9.52×10^{-7}
Mitotic cell cycle	146	1,184	1.11×10^{-6}
Proteinaceous extracellular matrix	82	578	1.36×10^{-6}
Organ morphogenesis	144	1,182	2.43×10^{-6}
Vasculature development	98	732	3.76×10^{-6}
Embryonic morphogenesis	96	728	7.04×10^{-6}
Cell proliferation	245	2,288	7.17×10^{-6}
Cell cycle	230	2,135	9.74×10^{-6}
Blood vessel development	93	707	1.31×10^{-5}
Response to wounding	191	1,738	2.02×10^{-5}
Receptor protein serine/threonine kinase signaling	56	369	2.12×10^{-5}
M phase of mitotic cell cycle	77	567	2.40×10^{-5}
Cell surface	86	671	3.26×10^{-5}
Organ development	362	3,675	3.68×10^{-5}
Collagen binding	21	90	3.90×10^{-5}
Glycosaminoglycan binding	42	262	4.65×10^{-5}
Mitotic spindle organization	12	33	7.15×10^{-5}
Cell adhesion	183	1,693	7.76×10^{-5}
Skeletal system morphogenesis	42	260	8.16×10^{-5}
Tissue development	185	1,720	8.76×10^{-5}
Cell surface receptor linked signaling pathway	368	3,785	8.98×10^{-5}
Mitosis	73	554	9.98×10^{-5}
Regulation of cell cycle	127	1,103	0.000109

on dishes coated with an AGI. CGNs isolated from newborn rats extended neurites on poly-L-lysine (PLL), but not on CSPG or MAG. Remarkably, both SHED-CM and DPSC-CM restored neurite extension activity of CGNs, while CM from fibroblasts (fibroblast-CM) or BMSCs (BMSC-CM) exhibited only subtle extension (Figure 5). Quantitative analysis showed that neurite extension through the inhibition of multiple AGIs was a unique characteristic of the tooth-derived stem cell (Figure 5, L and M). These results demonstrate that both SHEDs and DPSCs promote the regeneration of transected axons though direct inhibition of the multiple AGI signals by paracrine mechanisms.

SHEDs inhibited myelin degeneration. Next, we examined whether transplanted SHEDs preserved myelination in the transected SC by immunohistochemical staining with the fluorescent dye FluoroMyelin. In transverse sections of sham-operated SCs, white matter was clearly labeled by FluoroMyelin, and gray matter was not (data not shown). The control SCs exhibited little or no staining at the epicenter or 3 mm caudal to it (Figure 6, C and D). In contrast, we found significant FluoroMyelin-positive spots in the epicenter of the SHED-transplanted SCs, indicating that the SHEDs caused the regeneration of myelin structures in the transected region (Figure 6A). Notably, the myelin-positive areas of the SHED-transplanted SCs at 3 and 4 mm caudal to the epicenter constituted 55.3% ± 4.5% and 78.0% ± 4.1%, respectively, of the same areas in the sham-operated SCs, demonstrating that the SHEDs exerted remarkable myelin preservation activity (Figure 6E).

SHEDs survived and specifically differentiated into oligodendrocytes in the injured SC. In the FluoroMyelin-stained sections, we observed a myelin-expressing cell cluster in the gray matter of SHED-transplanted SCs (Figure 6B). We anticipated that these myelin-expressing cells would be mature oligodendrocytes derived from the transplanted SHEDs. To assess this possibility, we performed immunohistological analyses using anti–human nuclear antigen (HuNu) and two mature oligodendrocyte markers, APC and MBP (25, 26). Eight weeks after grafting, 32.3% ± 3.1% of the transplanted SHEDs still survived in the injured SCs (data not shown). Of these cells, 86.2% ± 6.2% and 90.2% ± 4.6% expressed APC and MBP, respectively (Figure 7). In addition, 10% of the HuNu-positive cells were negative for MBP and APC, but their fate is currently unknown (data not shown). Before the transplantation, SHEDs expressed many early neural cell lineage markers (Figure 1 and Table 1). However, the surviving transplanted SHEDs did not express NF-M or GFAP (Figure 7), indicating that they specifically differentiated along the oligodendrocyte lineage in the injured SCs.

SHEDs inhibited neuronal and glial apoptosis after SCI. SCI-induced cell death is a major contributor to secondary injury, in which irreversible tissue damage spreads across the SC. Twenty-four hours after injury, at 1 mm caudal to the epicenter, most of the cells expressing NeuN, GFAP, or MBP were costained with TUNEL, showing that massive multicellular apoptosis occurred immediately after SCI (Figure 8). The engrafted SHEDs significantly decreased the TUNEL staining in all 3 of these lineages (Figure 8, C, D, G, H, K, and L): The total number of TUNEL-positive cells in the SHED-transplanted SCs was approximately 20% of that in the control SCs (Figure 8M). The percentages of TUNEL-positive cells in the control and SHED-transplanted SCs were 87.7% ± 3.1% and 3.1% ± 3.2%, respectively (Figure 8N). These results demonstrate that the transplanted SHEDs minimized the expansion of secondary injury through strong neuroprotection of all the neural cell lineages.

Discussion

We report here the remarkable neuroregenerative activity of tooth-derived stem cells, SHEDs and DPSCs, for functional recovery after SCI. Previous studies have dealt with the differentiation characteristics of tooth-derived stem cells (16–19) and their trophic effects on the proliferation, migration, and survival of particular subsets of neurons (20–23). However, few studies have considered the therapeutic benefits of these stem cells for a particular neurological disorder. Our study revealed that engrafted SHEDs exhibited three major therapeutic benefits for recovery after SCI, including (a) inhibition of SCI-induced apoptosis of neurons, astrocytes, and oligodendrocytes, which promoted the preservation of neural fibers and myelin sheaths; (b) regeneration of the transected axon through the direct inhibition of multiple AGI signals, such as CSPGs and MAG,

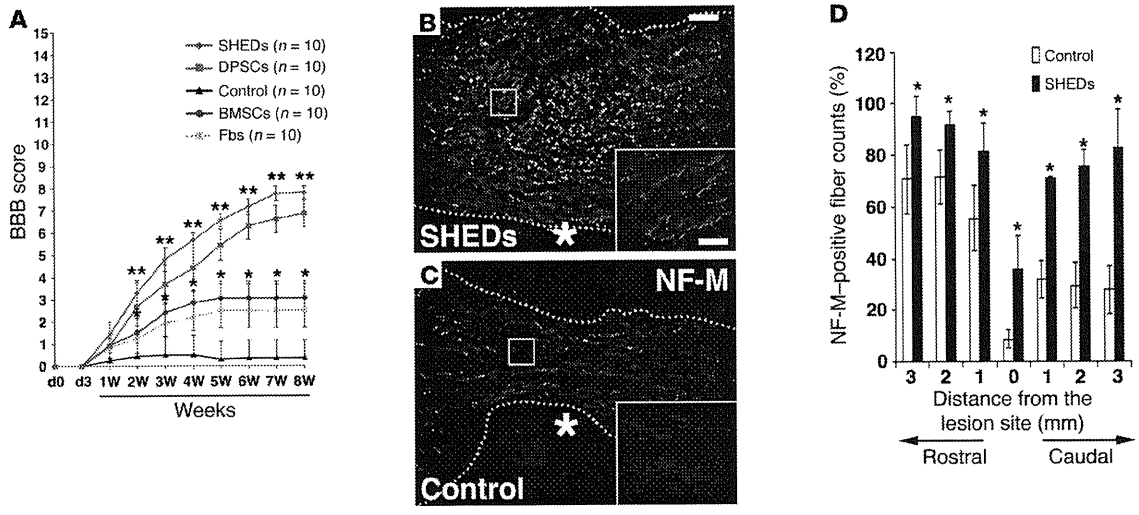

Figure 2

Engrafted SHEDs promote functional recovery of the completely transected SC. (**A**) Time course of functional recovery of hind limbs after complete transection of the SC. A total of 1 × 10^6 SHEDs, DPSCs, BMSCs, or fibroblasts were transplanted into the SCI immediately after transection. Data represent the mean ± SEM. $^{**}P < 0.001$, $^{*}P < 0.01$ compared with SCI models injected with PBS. (**B–D**) Representative images (**B** and **C**) and quantification (**D**) of NF-M–positive nerve fibers in sagittal sections of a completely transected SC, at 8 weeks after SCI. Dashed lines outline the SC. Insets are magnified images of boxed areas in **B** and **C**. (**D**) Nerve fiber quantification, representing the average of 3 experiments performed under the same conditions. The *x* axis indicates specific locations along the rostrocaudal axis of the SC (3 mm rostral and caudal to the epicenter), and *y* axis indicates the percentage of NF-M–positive fibers compared with that of the sham-operated SCs at the ninth thoracic spinal vertebrate (Th9) level. Data represent the mean ± SEM. $^{*}P < 0.05$ compared with SCI models injected with PBS. Scale bars: 100 μm and inset 20 μm (**B**) and 50 μm (**C**). Asterisks in **B** and **C** indicate the epicenter of the lesion.

by paracrine mechanisms; and (c) replacement of lost or damaged oligodendrocytes after SCI through specific differentiation into mature oligodendrocytes under the extreme conditions of SCI. To our knowledge, the latter two neuroregenerative activities (b and c) are unique to tooth-derived stem cells and are not exhibited by any other previously described stem cells. Thus, our data demonstrate that tooth-derived stem cells may provide significant therapeutic benefits for treating the acute phase of SCI through both cell-autonomous and paracrine/trophic regenerative activities.

Adult MSCs have been isolated from various tissues, including bone marrow, adipose tissue, skin, umbilical cord, and placenta (27–30). The therapeutic benefits of these stem cells have drawn intense attention in the field of translational medicine. Nevertheless, their biological equivalency/heterogeneity and identity are largely unknown (31). Tooth-derived stem cells exhibited BMSC-like multipotency and cell surface marker expression; however, they expressed a distinct set of multiple early neural linage markers (Table 1 and Figure 1). A cDNA microarray gene expression analysis showed that the SHEDs expressed many genes in the categories of extracellular and cell surface region, cell proliferation, and tissue/embryonic development, at levels at least 2-fold higher than BMSCs (Table 2). These data indicate that tooth-derived stem cells belong to a highly proliferative ectomesenchymal stem cell–like population that actively communicates with neighboring cells. These characteristics raise the question of what the role of these stem cells is in tooth development and maintenance. Although we do not have a clear answer at present, future analyses using model animals such as dogs and pigs may clarify their precise origin and normal functions, as well as identifying the physiological system that maintains the "stemness" of these cells in vivo.

Both axon regeneration and the reformation of appropriate neuronal connections are prerequisites for functional recovery from SCI. However, multiple AGIs block the inherent regenerative activities of injured axons (2–4). It is well known that multiple AGIs constitute a remarkably intricate molecular network in the extracellular space of the injured CNS, in which they activate a common intracellular signaling mediator, Rho GTPase, and its effector, Rho-associated kinase (ROCK) (32–36). The activation of the Rho-ROCK cascade induces growth cone collapse and axonal repulsion (37). The inactivation of Rho by C3 transferase or of ROCK by Y-27632 downregulates AGI signaling and promotes functional recovery after SCI (38–40). Thus, Rho/ROCK signaling is an important target for SCI treatments; however, no reports have yet described an effect of stem cell transplantation on regulating the multiple AGIs/Rho/ROCK signaling cascades. We found that engrafted SHEDs promoted the regeneration of two major types of descending axons (CST and 5-HT) beyond the lesion epicenter and concomitantly inhibited the SCI-induced Rho activation (Figure 4). Furthermore, both SHED-CM and DPSC-CM promoted the neurite extension of CGNs cultured on two different AGIs, CSPG and MAG (Figure 5). Taken together, these results strongly suggest that tooth-derived stem cells promote the regeneration of transected axons through the direct inhibition of multiple AGI signals by paracrine mechanisms. Notably, in contrast to the CMs from tooth-derived stem cells, BMSC-CM showed only a subtle anti-AGI activity in the neurite extension assay, in good agreement with the level of functional recovery observed in BMSC-transplanted rats. Thus, the anti-AGI activity of tooth-derived stem cells is one of their major therapeutic benefits for the treatment of SCI.

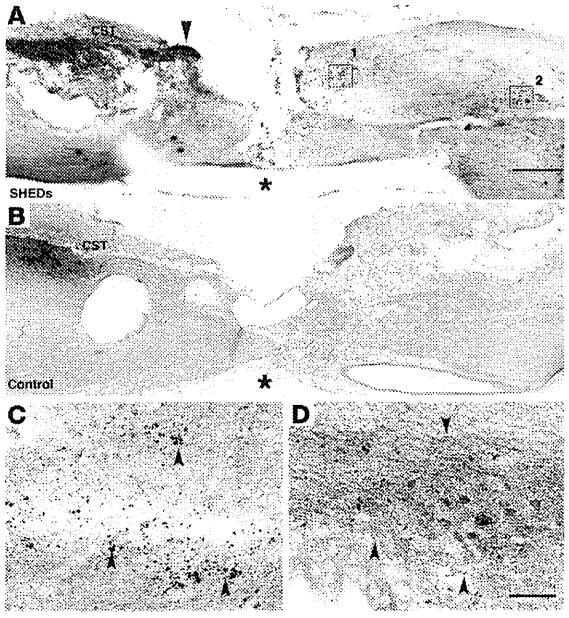

Figure 3
SHEDs regenerate CST fibers. Representative images of BDA-labeled CST axons. BDA-positive axons extended beyond the epicenter in the SHED-transplanted (**A**), but not the control SC (**B**). **C** and **D** are high-magnification views of boxed areas 1 and 2 in **A**, respectively. BDA-positive boutons were detected on the neurons of the caudal stump. Scale bars: 500 (**A**) and 100 μm (**D**). Arrowhead in **A** indicates abundant penetration of CST axons into the scar tissue of the rostral stump. Arrowheads in **C** and **D** indicate regenerated CST axons extended beyond the epicenter. Asterisks in **A** and **B** indicate the epicenter of the lesion.

The mechanisms that underlie the inhibition of multiple AGIs by SHED-CM and DPSC-CM are currently unknown. Although both SHEDs and DPSCs expressed an array of neurotrophic factors (Figure 1), our preliminary analysis showed that these trophic factors alone failed to promote the neurite extension of CGNs cultured on CSPG-coated dishes (K. Sakai and A. Yamamoto, unpublished observations). These results suggest that unknown factors, rather than neurotrophic factors, expressed by SHEDs and/or DPSCs may play major roles in the inhibition of multiple AGI signaling pathways. Since the strong anti-AGI activity was unique to the tooth-derived stem cells, but not to BMSCs, extracellular-related genes being preferentially expressed in SHEDs relative to BMSCs (Table 2) is a possible candidate anti-AGI factor. Future functional analysis of these genes will be required to reveal the molecular mechanisms by which tooth-derived stem cells regulate multiple AGI activities to promote the regeneration of injured axons.

It has been shown that pharmacological blockade of neuron and/or oligodendrocyte apoptosis by erythropoietin (41, 42), inhibitors of purine receptor P2X7 (OxATP and PPADS) (43), a neutralizing Ab against CD95 (FAS) antigen (44), or minocycline (45, 46) promotes functional recovery after SCI. We found that engrafted SHEDs suppressed the apoptosis of both neurons and oligodendrocytes (Figure 8), which resulted in the remarkable preservation of neurofilaments and myelin sheaths in the region surrounding the epicenter (Figures 2 and 6). Notably, in addition to these two cell lineages, SHEDs strongly inhibited the apoptosis of astrocytes recruited to the lesion. In the classical view, reactive, CSPG-generating astrocytes are considered to be an obstacle to axon regeneration; however, recent genetic studies in mice have shown that the conditional ablation of astrocytes after SCI resulted in larger lesions, failure of blood brain barrier repair, expansion of the inflammatory response and tissue disruption, severe demyelination, and profound cell death of neurons and oligodendrocytes (47–51). Thus, the accumulated evidence demonstrates that, in addition to their anti-regenerative activity, astrocytes play an important role in the neuroprotection during the acute phase of SCI. We found that SHEDs suppressed the apoptosis of astrocytes and minimized secondary injury but inhibited AGI activity of CSPG derived from activated astrocytes. Thus, these results demonstrate that SHEDs promote the neuroprotective role but inhibit the anti-neuroregenerative activity of astrocytes to promote functional recovery after SCI.

Figure 4
SHEDs regenerate 5-HT fibers and inhibit SCI-induced activation of Rho GTPase. (**A**–**D**) Representative images (**A**–**C**) and quantification (**D**) of serotonergic raphe axons stained with 5-HT mAb in the sagittal sections of the transected SC. A large number of 5-HT axons penetrated the scar tissue of the rostral stump in the SHED-transplanted SC (**A**), while only a few did in the control transected SC (**B**). (**C**) 5-HT–positive boutons were in contact with neurons of the caudal stump. Arrowhead indicates 5-HT–positive fiber extended beyond the epicenter. Quantification of regenerated 5-HT axons (**D**) was carried out as described in Figure 2D, except the *y* axis indicates the percentage of 5-HT axons compared with that in the sham-operated SC. Data represent the mean ± SEM. $^*P < 0.01$ compared with SCI models injected with PBS. Scale bars: 50 μm (**B** and **C**). (**E**) SCI-induced Rho GTPase activation 7 days after SCI was suppressed by engrafted SHEDs. The level of active Rho in lysate from the samples indicated at the top (sham-operated, control, and SHED-transplanted) was examined by RBD pull-down assay.

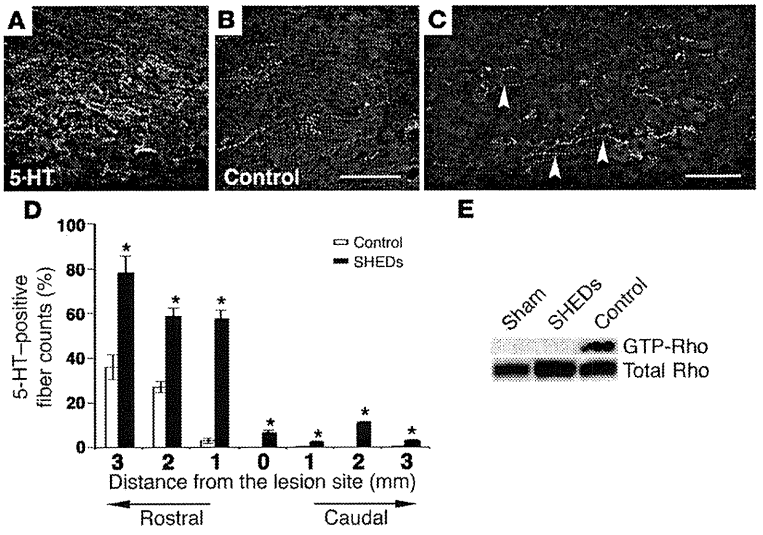

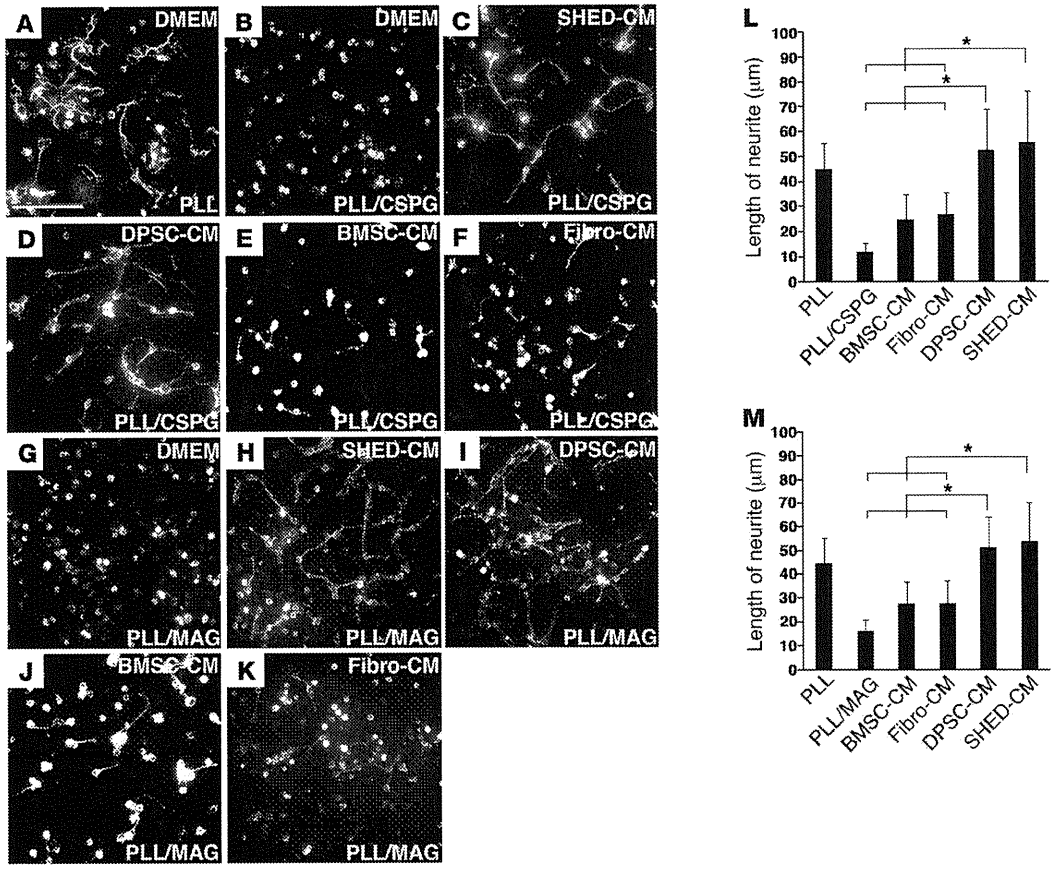

Figure 5

SHED-CM and DPSC-CM promote the neurite extension of CGNs on CSPG or MAG. CGNs were plated on PLL (**A**), PLL/CSPG (**B–F**), or PLL/MAG (**G–K**), with the CM indicated at the top of each panel. CGNs plated with SHED-CM or DPSC-CM extended their neurites on the CSPG- (**C** and **D**) and MAG-coated (**H** and **I**) dishes, while BMSC-CM and fibroblast-CM (Fibro-CM) elicited only marginal extension on CSPG (**E** and **F**) and MAG (**J** and **K**). Quantification of the neurite length of CGNs plated on CSPG (**L**) and MAG (**M**). The *y* axis indicates the neurite length. Data represent the average measurements for each cell type from 3 independent donors. This set of experiments was performed 3 times and yielded similar results. Error bars represent SD. $^*P < 0.05$. Scale bar in **A** is 100 μm.

Our data revealed two major advantages of using SHEDs for cell replacement in SCI treatment. First, we observed good survival of the engrafted SHEDs: more than 30% of the engrafted SHEDs survived as a cell mass in the injured SC. A previous study reported that, although the experimental details differed from ours, the survival rate of human ES cell–derived oligodendrocytes or motor neurons, transplanted just after complete SC transection, is less than 1% (8). We speculate that the SHED-mediated minimization of secondary injury and/or the formation of cohesive cell clusters of engrafted SHEDs may be attributable to their excellent cell survival rate. Second, we observed that the engrafted SHEDs specifically differentiated toward mature oligodendrocytes, expressing APC and MBP. It has been shown that DPSCs and SHEDs differentiate in vitro toward functionally active neurons that express voltage-gated Na^+ channels and in vivo toward neuron-like cells 48 hours after their transplantation into the mesencephalon of avian embryos (18). Taken together with our findings, these results support the idea that tooth-derived stem cells exhibit neural stem cell–like characteristics and that unknown environmental cues are important for their fate determination. Since cell-based remyelination strategies can restore saltatory conduction and promote functional recovery after SCI (52), the SHED's strong cell survival and oligodendrocyte-specific differentiation potential, particularly under the extreme conditions of SCI, would be great advantages in using these cells to treat SCI. It is hoped that in the future, clarification of the regulatory cues for the specific differentiation of SHEDs will help us to establish efficient therapeutic protocols for SCI patients based on precise cell fate control.

The aim of this study was to address the neuroregenerative activity of tooth-derived stem cells in a particular CNS injury model, SCI. We used the rat complete transection model, because it provides good reproducibility and permits a more accurate assessment of the effects of treatment than do other SCI models. Although contusion and crush models would provide experimental conditions that are closer to the SCIs seen clinically in humans, the amount of injury in these models is not consistent from animal to animal. Furthermore, these incomplete transection models permit spontaneous recovery after SCI, and the residual SC tissues may provide routes for the compensatory sprouting of uninjured SC axons (53). Thus, the transection model was cho-

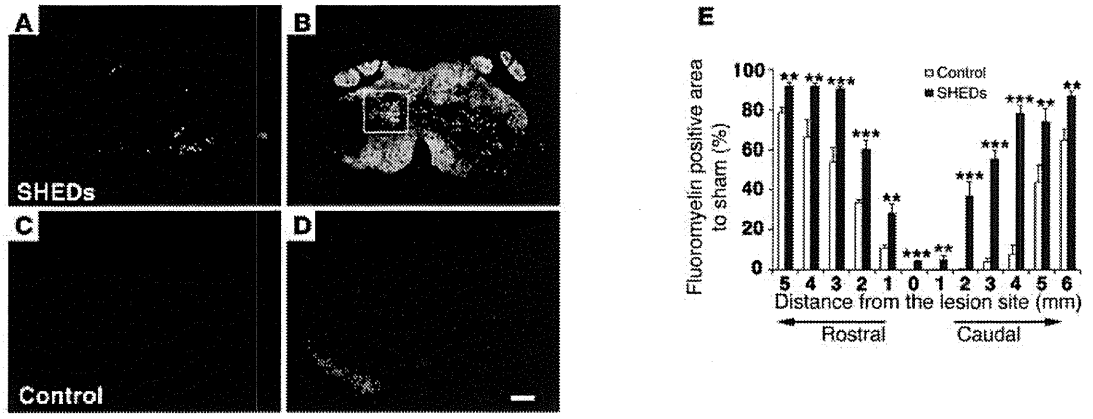

Figure 6
SHEDs preserve myelin sheath and differentiate into mature oligodendrocytes in the transected SC. Representative images (**A**–**D**) and quantification (**E**) of the myelinated area 8 weeks after SCI. Transverse sections of the epicenter (**A** and **C**) and 3 mm caudal to it (**B** and **D**) were stained with FluoroMyelin. The myelinated area in both regions was significantly preserved in the SHED-transplanted SC (**A** and **B**), but abolished in the control SC (**C** and **D**). Scale bar: 100 μm (**D**). (**E**) Quantification of the myelinated area showing the average of 3 experiments performed in parallel. The *x* axis indicates specific locations along the rostrocaudal axis of the SC. The *y* axis indicates the percentage of the myelin-positive area compared with that of the sham-operated SC at the Th9 level. Error bars represent SD. $^{**}P < 0.01$, $^{***}P < 0.001$ compared with SCI models injected with PBS.

sen as most appropriate for the precise assessment of the axonal regeneration activity of tooth-derived stem cells.

In this study, we transplanted cells into the injured SC immediately after surgical transection, which is impractical for most human SCI cases. We chose this system to examine the therapeutic benefits of the transplanted cells in countering the multiple pathogenic signals that function synergistically during the early phase of SCI. Our future studies will analyze the neuroregenerative activities of tooth-derived stem cells in SCI under more clinically relevant experimental conditions.

In conclusion, we demonstrated multifaceted neuroregenerative activities of tooth-derived stem cells that fulfill many requirements for functional recovery after SCI. Not only did engrafted SHEDs have remarkable neuroregenerative activities, they also showed no malignant transformation 8 weeks after implantation (data not shown). Furthermore, SHEDs and DPSCs can be obtained from exfoliated deciduous and impacted adult wisdom teeth without adverse health effects. Thus, there are few ethical concerns regarding their clinical use. We propose that tooth-derived stem cells may be an excellent and practical cellular resource for the treatment of SCI.

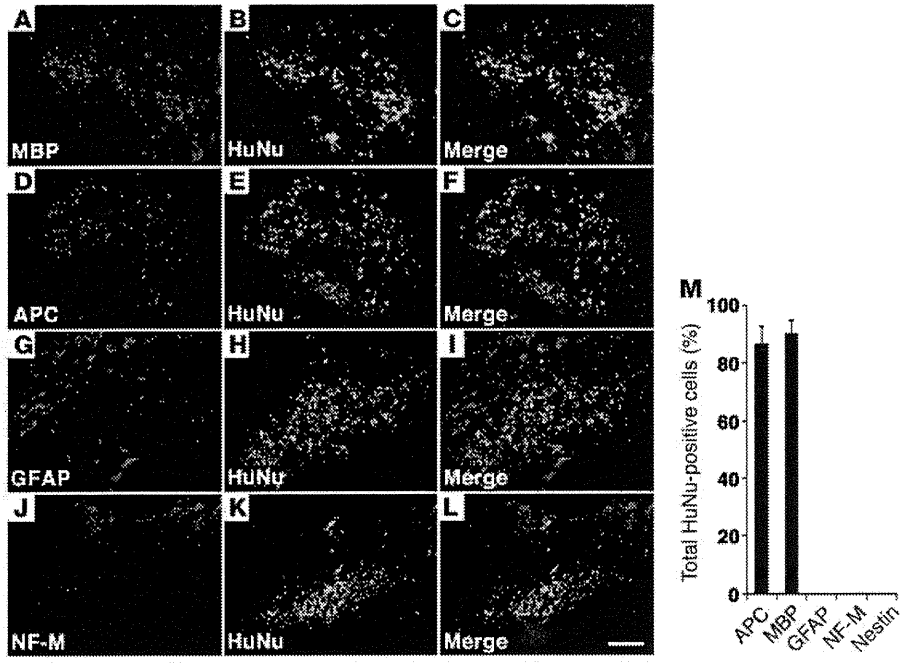

Figure 7
SHEDs differentiate into mature oligodendrocytes in the transected SC. A myelin-positive cell cluster ectopically identified in the medulla of a SHED-transplanted SC (boxed area in Figure 6B) was characterized by immunohistochemical staining with an anti–human nuclei mAb (HuNu) together with Abs against neural cell lineage markers: anti-MBP (**A**–**C**), anti-APC (**D**–**F**), anti-GFAP (**G**–**I**), or anti–NF-M (**J**–**L**). The data indicate that SHEDs specifically differentiate into mature oligodendrocytes. The percentage of the lineage marker–positive to total HuNu-positive cell number (**M**) represents the average of 3 experiments performed in parallel. Error bars represent SD. Scale bar: 100 μm (**L**).

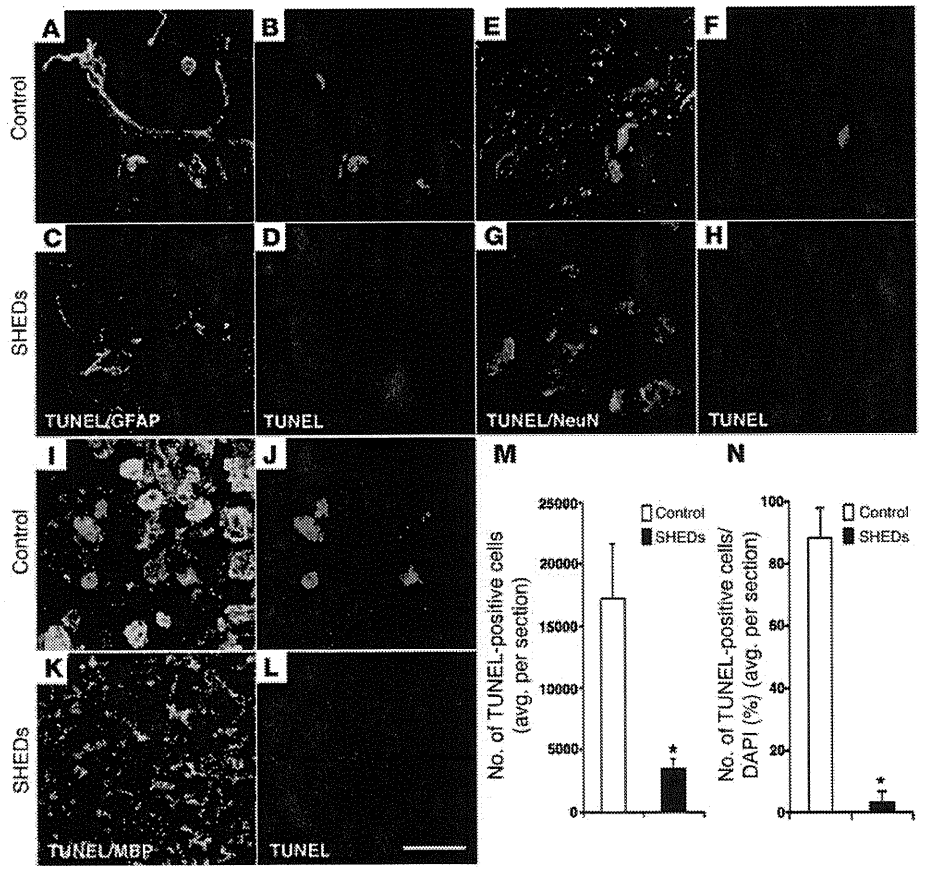

Figure 8
SHEDs suppress the apoptosis of neural cell lineages and secondary injury after SCI. Representative images (**A**–**L**) and quantifications (**M** and **N**) of apoptotic cell death 24 hours after SCI. Transverse sections 1 mm caudal to the epicenter of PBS-injected (**A**, **B**, **E**, **F**, **I**, and **J**) and SHED-transplanted SCs (**C**, **D**, **G**, **H**, **K**, and **L**) were stained with TUNEL and then subjected to immunohistochemical analysis with an anti-GFAP mAb (**A**–**D**), anti-NeuN mAb (**E**–**H**), or anti-MBP mAb (**I**–**L**). The engrafted SHEDs decreased the apoptotic cell death of all 3 neural cell lineages. (**M**) Quantification of the total TUNEL-positive cell number within 3 mm rostral and caudal to the epicenter shows the average of 3 experiments performed in parallel. (**N**) The percentage of TUNEL-positive relative to total DAPI-positive cell number in the same area as in **M**. Error bars represent SD. $^*P < 0.01$ compared with SCI models injected with PBS. Scale bar: 20 μm (**L**).

Methods

Isolation of SHEDs and DPSCs, and cell culture. Human SHEDs and DPSCs were isolated as described previously (16, 17). Briefly, exfoliated deciduous teeth (from individuals 6–12 years old) and adult third molars (18–30 years old) extracted for clinical purposes were collected. After separation of the crown and root, the dental pulp was isolated and then digested in a solution of 3 mg/ml collagenase type I and 4 mg/ml dispase for 1 hour at 37°C. Single-cell suspensions (1×10^4 to 2×10^4 cells/ml) were plated on culture dishes in DMEM supplemented with 10% fetal calf serum, then incubated at 37°C in 5% CO_2. Mesenchymal stem cells of three human bone marrow lines (hBMSCs, from individuals 20–22 years old) at passage 5 and three human skin-fibroblast lines (hFbs, 36–40-years old) at passage 5 were obtained from Lonza and the Health Science Research Resources Bank Japan, respectively.

Real-time PCR and microarray analysis. Total RNA was quantified by a spectrophotometer, and RNA integrity was checked on 1% agarose gels. RT reactions were carried out with Superscript III reverse transcriptase (Invitrogen) using 1 μg of total RNA in a 50 μl total reaction volume. Real-time PCR was performed using the THUNDERBIRD SYBR qPCR Mix (Toyobo) driven by the StepOnePlus Real-Time PCR System (Applied Biosystems). Primers were designed using DNADynamo (BlueTractorSoftware Ltd) and primer 3, as follows: *BDNF* forward (5′-GGGAAAAGGGAACAGGAAAA-3′), *BDNF* reverse (5′-AACAGACAGGATGGGCAGAA-3′), *GDNF* forward (5′-CGAACTCTTGCCCCTGACCT-3′), *GDNF* reverse (5′-ACAGCCACGACATCCCATAAC-3′), *CNTF* forward (5′-CCTTCTCTCTTCCTTGCTTTCTCTT-3′), *CNTF* reverse (5′-TGTCCCTGCTCCCACTCTCT-3′), *NT-3* forward (5′-TCAAAACGGGCAACTCTCCT-3′), *NT-3* reverse (5′-CTCGACAAGGCACACACACA-3′), *NGF* forward (5′-TTCCCTTGACACTGCCCTTC-3′), *NGF* reverse (5′-GATGATGACCGCTTGCTCCT-3′). Microarray experiments were carried out using a CodeLink Human Whole Genome Bioarray (Applied Microarrays Inc.) at Filgen Inc. The arrays were scanned using a GenePix4000B Array Scanner (Molecular Devices). The data were analyzed by using MicroArray Data Analysis Tool version 3.2 (Filgen Inc.) and deposited in the GEO database (accession GSE32403).

Flow cytometry analysis. For flow cytometry, 1×10^6 cells were incubated with FITC-conjugated primary mAbs against CD34, CD45, and CD11b and PE-conjugated against HLA-DR, CD105, CD73, and CD90 (BD Biosciences) at 4°C for 30 minutes and then washed twice with PBS containing 0.1% bovine serum albumin. The expression of intracellular markers was examined by indirect immunostaining. Cells were fixed with 4% (w/v) PFA for 5 minutes and permeabilized with 0.1% (v/v) Triton X-100 in PBS for 5 minutes. After blocking with 10% (v/v) goat serum for 30 minutes, the cells were incubated with primary Abs: anti-GFAP (mouse IgG, 1:500, Millipore), anti-βIII-tubulin (mouse IgG, 1:1,000, R&D Systems), anti-NeuN (mouse IgG, 1:100, Millipore), anti-CNPase (mouse IgG, 1:500, Millipore), anti-nestin (rabbit IgG, 1:500, Millipore), anti-DCX (guinea pig IgG, 1:500, Millipore), anti-APC (rabbit IgG, 1:300, Abcam), anti-MBP (rabbit IgG, 1:500, Abcam), anti-A2B5 mAb (mouse IgG, 1:500, Millipore). The secondary Abs were anti-mouse IgG, anti-rabbit IgG, and anti-guinea pig IgG-conjugated with Alexa Fluor 448 (Invitrogen), used at 1:1,000. Cell fluorescence was evaluated by flow cytometry using a FACSCalibur (BD Biosciences).

Animal model and surgical procedure. Adult female Sprague-Dawley rats were anesthetized with a mixture of xylazine (100–150 mg/kg) and ketamine (60–90 mg/kg). After laminectomy at the 9th–11th thoracic vertebral lev-

els, the dura was opened, and the SC was completely transected using a surgical blade (Feather surgical blade stainless steel no. 11). The severed ends of the SCs typically retracted about 1–2 mm. The rostral and caudal stumps were lifted to ensure complete transection. Then, 1×10^6 cells were drawn into a glass pipette with a tip diameter of 50–70 mm mounted onto a 10-μl Hamilton syringe attached to a micromanipulator. First, the cells were deposited into two injection sites at the rostral and the caudal stumps, 2 mm from the lesion and 0.5 mm lateral to the midline, at a depth of 1.5 mm. A 2.5-μl sample containing 2.5×10^5 cells in PBS was grafted into each site (injection rate, 0.8 μl/min). Next, 1×10^5 cells in fibrin glue were implanted into the 1- to 2-mm gap to fill the lesion site in the severed SC. After surgery, the rats were placed in temperature- and humidity-controlled incubation chambers until they awoke. They were then transferred to cages, and bladder evacuation was applied daily. Antibiotics (sodium ampicillin, 10 mg/kg body weight) were injected into the rats daily for a week. The rats were maintained under postoperative care for 8 weeks. All rats were given cyclosporine (Novartis) at 10 mg/kg/d on the day before surgery transplantation, then every day after surgery.

Immunohistochemical analysis. Cells were plated on PLL-coated 8-chamber slides and then incubated with the primary Abs listed above. For histological examination of the treated SCs, the animals were anesthetized and transcardially perfused with 4% PFA in 0.1 M PBS, 8 weeks after transplantation. The SCs were embedded in OCT compound (Sakura Finetek) and sectioned in the sagittal or transverse plane at 20 μm on a cryostat (Leica). The sections were incubated with primary Abs against human nuclei (mouse IgG, 1:100), NF-M (rabbit IgG, 1:300, Millipore), and 5-HT (rabbit IgG, 1:500, Sigma-Aldrich) in addition to the Abs listed above. Secondary Abs were anti-mouse IgG–Alexa Fluor 488, anti-rabbit IgG–Alexa 546, and anti–guinea pig IgG–Alexa 647. Myelin was stained by FluoroMyelin green dye (Invitrogen), according to the manufacturer's instructions. After counterstaining with DAPI (Sigma-Aldrich), cell images were captured with a confocal laser scanning microscope (A1Rsi, Nikon), while tissue images were taken with a universal fluorescence microscope (BZ9000, Keyence).

The differentiation activity of the engrafted SHEDs and the cells staining positive for MBP, APC, NF-M, or GFAP among the anti-human nuclei–positive transplanted cells were quantified. Cells were counted in at least 15 confocal images from 3 individuals in parallel experiments, with error bars representing SD.

Anterograde neuronal tracing study. For tracing of the CSTs, 0.5 μl of 5% biotinylated dextran amine (BDA: MW 10,000, Molecular Probes, Invitrogen; 5% in PBS) was injected into 4 sites in the hind limb area of the sensorimotor cortex at a 1.2-mm depth, following the rat brain atlas (54). Two weeks after the injections, sagittal cryosections (20 μm thick) of the SCs were prepared and processed by diaminobenzidine (DAB) staining with the ABC reaction protocol (VECTASTAIN Elite ABC, Vector Laboratories).

BBB open field locomotor score. Hind limb neurobehavioral testing was performed using the BBB locomotor rating scale (24). The 22-point (from 0 to 21) BBB scale was used to assess hind limb locomotor recovery, including joint movements, stepping ability, coordination, and trunk stability. A score of 21 indicates unimpaired locomotion as observed in uninjured rats. Two examiners who were blinded to the animal's treatments performed the tests. The duration of each session was 4 minutes per rat. The scores were analyzed by repeated-measures ANOVA with Tukey's multiple comparison tests at each time point.

CM. At 70%–80% confluence, the cell culture medium was changed to serum-free DMEM. After 48 hours incubation at 37°C in 5% CO_2, the CM was collected and centrifuged for 4–5 minutes at 4°C, 22,140 *g*. After the brief re-centrifugation, the supernatant was collected and used as CM.

Neurite outgrowth assays. Forty-eight-well tissue culture plates (Falcon, BD) were coated with 20 μg/ml PLL (Sigma-Aldrich) and then with 300 ng/ml extracellular CSPG mixture (Millipore) or 400 ng/ml MAG/Fc Chimera (MAG; Sigma-Aldrich) for 4 hours at 37°C. Rat CGNs were seeded onto PLL-, PLL/CSPG-, or PLL/MAG-coated 48-well tissue culture plates at 2.0×10^4 cells/well and cultured at 37°C in 5% CO_2 with SHED-CM, DPSC-CM, BMSC-CM, or fibroblast-CM. After 24 hours incubation, cells were fixed in 4% paraformaldehyde/PBS and stained with anti-neuron-specific βIII-tubulin (R&D Systems) to visualize neurites. Cell processes were defined as neurites when they were longer than the diameter of the cell body. Neurite length was evaluated by manually tracing neurite per cell using ImageJ software (version 1.29, http://rsbweb.nih.gov/ij/) and referenced to a known length. Each experiment was conducted in triplicate, and images were taken with 20 or more cells per field. For each experiment, at least 100 cells were randomly counted and measured.

Analysis of apoptosis. Apoptotic cell death was analyzed by TUNEL assay (In Situ Cell Death Detection kit, Roche). TUNEL-positive cells were counted on sections from sham-treated, PBS-injected, and SHED-transplanted animals. A researcher blinded to the experimental protocol determined the number of TUNEL-positive cells in the entire serial parasagittal section. The average number of TUNEL-positive cells per section was calculated from the values obtained by counting serial sagittal sections through the lesion site of each animal, with 3 animals examined per group.

Statistics. An unpaired 2-tailed Student's *t* test was used for single comparisons. For analysis of the real-time PCR results and open-field scores, we used repeated-measures ANOVA with Tukey's post hoc test (SPSS 19.0). A *P* value less than 0.05 was considered significant.

Study approval. The animal studies were carried out in accordance with the NIH Guidelines for the Care and Use of Laboratory Animals and approved by the Animal Research Committee of Nagoya University. Extracted teeth were collected at the Nagoya University School of Medicine, under approved guidelines set by Nagoya University (H-73, 2003). Ethical approval was obtained from the ethics committee of Nagoya University (permission number 8-2). All participants provided written informed consent.

Acknowledgments

We are grateful to T. Yamashita (Osaka University) and M. Hibi (Nagoya University) for critical reading of the manuscript. We also thank T. Isa and T. Umeda (National Institute for Physiological Sciences); M. Koda and H. Takahashi (Chiba University); and M. Abematsu (Kagoshima University) for technical instruction. We are grateful to M. Fujio and R. Shohara for their comments and support of this study. We thank the Division of Experimental Animals and Medical Research Engineering, Nagoya University Graduate School of Medicine, for the housing of mice and for microscope maintenance. This work was supported by Grants-in-Aid for Scientific Research on Priority Areas from the Ministry of Education, Culture, Sports, Science and Technology of Japan; Grants-in-Aid for Practical Application of Regenerative Medicine from the Ministry of Health, Labour and Welfare of Japan; and COE for education and research of Micro-Nano Mechatronics Nagoya University Global COE Program.

Received for publication May 31, 2011, and accepted in revised form October 12, 2011.

Address correspondence to: Akihito Yamamoto, Department of Oral and Maxillofacial Surgery, Nagoya University Graduate School of Medicine, 65 Tsurumai-cho, Showa-ku, Nagoya 466-8550, Japan. Phone: 81.52.744.1978; Fax: 81.52.744.1978; E-mail: akihito@med.nagoya-u.ac.jp.

1. Norenberg MD, Smith J, Marcillo A. The pathology of human spinal cord injury: defining the problems. *J Neurotrauma.* 2004;21(4):429–440.
2. Schwab JM, et al. Experimental strategies to promote spinal cord regeneration — an integrative perspective. *Prog Neurobiol.* 2006;78(2):91–116.
3. Rowland JW, Hawryluk GW, Kwon B, Fehlings MG. Current status of acute spinal cord injury pathophysiology and emerging therapies: promise on the horizon. *Neurosurg Focus.* 2008;25(5):E2.
4. Yiu G, He Z. Glial inhibition of CNS axon regeneration. *Nat Rev Neurosci.* 2006;7(8):617–627.
5. Cummings BJ, et al. Human neural stem cells differentiate and promote locomotor recovery in spinal cord-injured mice. *Proc Natl Acad Sci U S A.* 2005; 102(39):14069–14074.
6. Keirstead H, et al. Human embryonic stem cell-derived oligodendrocyte progenitor cell transplants remyelinate and restore locomotion after spinal cord injury. *J Neurosci.* 2005;25(19):4694–4705.
7. Kumagai G, et al. Roles of ES cell-derived gliogenic neural stem/progenitor cells in functional recovery after spinal cord injury. *PLoS One.* 2009;4(11):e7706.
8. Erceg S, et al. Transplanted oligodendrocytes and motoneuron progenitors generated from human embryonic stem cells promote locomotor recovery after spinal cord transection. *Stem Cells.* 2010; 28(9):1541–1549.
9. Hofstetter CP, et al. Marrow stromal cells form guiding strands in the injured spinal cord and promote recovery. *Proc Natl Acad Sci U S A.* 2002; 99(4):2199–2204.
10. Cizkova D, Rosocha J, Vanicky I, Jergova S, Cizek M. Transplants of human mesenchymal stem cells improve functional recovery after spinal cord injury in the rat. *Cell Mol Neurobiol.* 2006; 26(7–8):1167–1180.
11. Sharp J, Keirstead HS. Therapeutic applications of oligodendrocyte precursors derived from human embryonic stem cells. *Curr Opin Biotechnol.* 2007; 18(5):434–440.
12. Deshpande DM, et al. Recovery from paralysis in adult rats using embryonic stem cells. *Ann Neurol.* 2006;60(1):32–44.
13. Kopen GC, Prockop DJ, Phinney DG. Marrow stromal cells migrate throughout forebrain and cerebellum, and they differentiate into astrocytes after injection into neonatal mouse brains. *Proc Natl Acad Sci U S A.* 1999;96(19):10711–10716.
14. Furuya T, et al. Treatment of rat spinal cord injury with a Rho-kinase inhibitor and bone marrow stromal cell transplantation. *Brain Res.* 2009; 1295:192–202.
15. Gronthos S, et al. Stem cell properties of human dental pulp stem cells. *J Dent Res.* 2002;81(8):531–535.
16. Gronthos S, Mankani M, Brahim J, Robey PG, Shi S. Postnatal human dental pulp stem cells (DPSCs) in vitro and in vivo. *Proc Natl Acad Sci U S A.* 2000;97(25):13625–13630.
17. Miura M, et al. SHED: stem cells from human exfoliated deciduous teeth. *Proc Natl Acad Sci U S A.* 2003;100(10):5807–5812.
18. Arthur A, Rychkov G, Shi S, Koblar SA, Gronthos S. Adult human dental pulp stem cells differentiate toward functionally active neurons under appropriate environmental cues. *Stem Cells.* 2008; 26(7):1787–1795.
19. Wang J, et al. Stem cells from human-exfoliated deciduous teeth can differentiate into dopaminergic neuron-like cells. *Stem Cells Dev.* 2010; 19(9):1375–1383.
20. Nosrat IV, Widenfalk J, Olson L, Nosrat CA. Dental pulp cells produce neurotrophic factors, interact with trigeminal neurons in vitro, and rescue motoneurons after spinal cord injury. *Dev Biol.* 2001; 238(1):120–132.
21. Nosrat IV, Smith CA, Mullally P, Olson L, Nosrat CA. Dental pulp cells provide neurotrophic support for dopaminergic neurons and differentiate into neurons in vitro; implications for tissue engineering and repair in the nervous system. *Eur J Neurosci.* 2004;19(9):2388–2398.
22. Huang AH-C, Snyder BR, Cheng P-H, Chan AWS. Putative dental pulp-derived stem/stromal cells promote proliferation and differentiation of endogenous neural cells in the hippocampus of mice. *Stem Cells.* 2008;26(10):2654–2663.
23. Arthur A, Shi S, Zannettino AC, Fujii N, Gronthos S, Koblar SA. Implanted adult human dental pulp stem cells induce endogenous axon guidance. *Stem Cells.* 2009;27(9):2229–2237.
24. Basso DM, Beattie MS, Bresnahan JC. A sensitive and reliable locomotor rating scale for open field testing in rats. *J Neurotrauma.* 1995;12(1):1–21.
25. Mirsky R, Winter J, Abney ER, Pruss RM, Gavrilovic J, Raff MC. Myelin-specific proteins and glycolipids in rat Schwann cells and oligodendrocytes in culture. *J Cell Biol.* 1980;84(3):483–494.
26. Bhat RV, et al. Expression of the APC tumor suppressor protein in oligodendroglia. *Glia.* 1996; 17(2):169–174.
27. In 't Anker PS, et al. Isolation of mesenchymal stem cells of fetal or maternal origin from human placenta. *Stem Cells.* 2004;22(7):1338–1345.
28. Romanov YA, Svintsitskaya VA, Smirnov VN. Searching for alternative sources of postnatal human mesenchymal stem cells: candidate MSC-like cells from umbilical cord. *Stem Cells.* 2003; 21(1):105–110.
29. Young HE, et al. Human reserve pluripotent mesenchymal stem cells are present in the connective tissues of skeletal muscle and dermis derived from fetal, adult, and geriatric donors. *Anat Rec.* 2001; 264(1):51–62.
30. Zuk PA, et al. Human adipose tissue is a source of multipotent stem cells. *Mol Biol Cell.* 2002; 13(12):4279–4295.
31. Nombela-Arrieta C, Ritz J, Silberstein LE. The elusive nature and function of mesenchymal stem cells. *Nat Rev Mol Cell Biol.* 2011;12(2):126–131.
32. Maekawa M, et al. Signaling from Rho to the actin cytoskeleton through protein kinases ROCK and LIM-kinase. *Science.* 1999;285(5429):895–898.
33. Winton MJ, Dubreuil CI, Lasko D, Leclerc N, McKerracher L. Characterization of new cell permeable C3-like proteins that inactivate Rho and stimulate neurite outgrowth on inhibitory substrates. *J Biol Chem.* 2002;277(36):32820–32829.
34. Yamashita T, Tohyama M. The p75 receptor acts as a displacement factor that releases Rho from Rho-GDI. *Nat Neurosci.* 2003;6(5):461–467.
35. Monnier PP, Sierra A, Schwab JM, Henke-Fahle S, Mueller BK. The Rho/ROCK pathway mediates neurite growth-inhibitory activity associated with the chondroitin sulfate proteoglycans of the CNS glial scar. *Mol Cell Neurosci.* 2003;22(3):319–330.
36. Dubreuil C, Winton M, McKerracher L. Rho activation patterns after spinal cord injury and the role of activated Rho in apoptosis in the central nervous system. *J Cell Biol.* 2003;162(2):233–243.
37. Hall A. Rho GTPases and the actin cytoskeleton. *Science.* 1998;279(5350):509–514.
38. Lehmann M, et al. Inactivation of Rho signaling pathway promotes CNS axon regeneration. *J Neurosci.* 1999;19(17):7537–7547.
39. Dergham P, Ellezam B, Essagian C, Avedissian H, Lubell WD, McKerracher L. Rho signaling pathway targeted to promote spinal cord repair. *J Neurosci.* 2002; 22(15):6570–6577.
40. Fournier AE, Takizawa BT, Strittmatter SM. Rho kinase inhibition enhances axonal regeneration in the injured CNS. *J Neurosci.* 2003;23(4):1416–1423.
41. Celik M, et al. Erythropoietin prevents motor neuron apoptosis and neurologic disability in experimental spinal cord ischemic injury. *Proc Natl Acad Sci U S A.* 2002;99(4):2258–2263.
42. Gorio A, et al. Recombinant human erythropoietin counteracts secondary injury and markedly enhances neurological recovery from experimental spinal cord trauma. *Proc Natl Acad Sci U S A.* 2002; 99(14):9450–9455.
43. Wang X, et al. P2X7 receptor inhibition improves recovery after spinal cord injury. *Nature Med.* 2004; 10(8):821–827.
44. Demjen D, et al. Neutralization of CD95 ligand promotes regeneration and functional recovery after spinal cord injury. *Nature Med.* 2004;10(4):389–395.
45. Stirling DP, et al. Minocycline treatment reduces delayed oligodendrocyte death, attenuates axonal dieback, and improves functional outcome after spinal cord injury. *J Neurosci.* 2004;24(9):2182–2190.
46. Teng YD, et al. Minocycline inhibits contusion-triggered mitochondrial cytochrome c release and mitigates functional deficits after spinal cord injury. *Proc Natl Acad Sci U S A.* 2004;101(9):3071–3076.
47. Bush TG, et al. Leukocyte infiltration, neuronal degeneration, and neurite outgrowth after ablation of scar-forming, reactive astrocytes in adult transgenic mice. *Neuron.* 1999;23(2):297–308.
48. Faulkner JR, Herrmann JE, Woo MJ, Tansey KE, Doan NB, Sofroniew MV. Reactive astrocytes protect tissue and preserve function after spinal cord injury. *J Neurosci.* 2004;24(9):2143–2155.
49. Okada S, et al. Conditional ablation of Stat3 or Socs3 discloses a dual role for reactive astrocytes after spinal cord injury. *Nature Med.* 2006; 12(7):829–834.
50. Herrmann JE, et al. STAT3 is a critical regulator of astrogliosis and scar formation after spinal cord injury. *J Neurosci.* 2008;28(28):7231–7243.
51. Rolls A, Shechter R, Schwartz M. The bright side of the glial scar in CNS repair. *Nat Rev Neurosci.* 2009;10(3):235–241.
52. Keirstead HS. Stem cells for the treatment of myelin loss. *Trends Neurosci.* 2005;28(12):677–683.
53. Thuret S, Moon LDF, Gage FH. Therapeutic interventions after spinal cord injury. *Nat Rev Neurosci.* 2006;7(8):628–643.
54. Paxinos G, Watson C. *The Rat Brain in Stereotaxic Coordinates.* 2nd ed. Orlando, Florida, USA: Academic Press; 1986.

THE JOURNAL OF BIOLOGICAL CHEMISTRY VOL. 286, NO. 36, pp. 31337–31346, September 9, 2011

Specific Enzyme Complex of β-1,4-Galactosyltransferase-II and Glucuronyltransferase-P Facilitates Biosynthesis of *N*-linked Human Natural Killer-1 (HNK-1) Carbohydrate*[S]

Received for publication, February 21, 2011, and in revised form, July 5, 2011 Published, JBC Papers in Press, July 19, 2011, DOI 10.1074/jbc.M111.233353

Tetsuya Kouno[‡], Yasuhiko Kizuka[§1], Naoki Nakagawa[‡], Toru Yoshihara[¶‖], Masahide Asano[¶], and Shogo Oka[‡2]

From the [‡]Department of Biological Chemistry, Human Health Sciences, Graduate School of Medicine, and [§]Department of Biological Chemistry, Graduate School of Pharmaceutical Sciences, Kyoto University, Kyoto 606-8507 and the [¶]Division of Transgenic Animal Science, Advanced Science Research Center, and [‖]Research Center for Child Mental Development, Kanazawa University, Kanazawa 920 8640, Japan

Human natural killer-1 (HNK-1) carbohydrate is highly expressed in the nervous system and is involved in synaptic plasticity and dendritic spine maturation. This unique carbohydrate, consisting of a sulfated trisaccharide (HSO_3-3GlcAβ1–3Galβ1–4GlcNAc-), is biosynthesized by the successive actions of β-1,4-galactosyltransferase (β4GalT), glucuronyltransferase (GlcAT-P and GlcAT-S), and sulfotransferase (HNK-1ST). A previous study showed that mice lacking β4GalT-II, one of seven β4GalTs, exhibited a dramatic loss of HNK-1 expression in the brain, although β4GalT-I-deficient mice did not. Here, we investigated the underlying molecular mechanism of the regulation of HNK-1 expression. First, focusing on a major HNK-1 carrier, neural cell adhesion molecule, we found that reduced expression of an *N*-linked HNK-1 carbohydrate caused by a deficiency of β4GalT-II is not likely due to a general loss of the β1,4-galactose residue as an acceptor for GlcAT-P. Instead, we demonstrated by co-immunoprecipitation and endoplasmic reticulum-retention analyses using Neuro2a (N2a) cells that β4GalT-II physically and specifically associates with GlcAT-P. In addition, we revealed by pull-down assay that Golgi luminal domains of β4GalT-II and GlcAT-P are sufficient for the complex to form. With an *in vitro* assay system, we produced the evidence that the kinetic efficiency k_{cat}/K_m of GlcAT-P in the presence of β4GalT-II was increased about 2.5-fold compared with that in the absence of β4GalT-II. Finally, we showed that co-expression of β4GalT-II and GlcAT-P increased HNK-1 expression on various glycoproteins in N2a cells, including neural cell adhesion molecule. These results indicate that the specific enzyme complex of β4GalT-II with GlcAT-P plays an important role in the biosynthesis of HNK-1 carbohydrate.

Glycosylation is a major post-translational modification, especially for cell surface and extracellular proteins, and plays important roles in cellular functions such as adhesion, endocytosis, and receptor signaling (1, 2). In general, glycan is biosynthesized in a stepwise manner by ER[3]- or Golgi-resident glycosyltransferases. As most of these glycosyltransferases have been cloned, there is an overall understanding of the pathway of production. However, the expression of a given glycosyltransferase does not always reflect that of its product, because it has become clear that activities of glycosyltransferases are regulated by oligomerization or proteolytic cleavage (3, 4). In addition, some glycosyltransferases form heterocomplexes that alter their activities, substrate specificity, or distribution in the ER or Golgi apparatus (5, 6). Thus, to understand the functions and biosynthesis of glycans, it is necessary to clarify how the activity of individual glycosyltransferases is regulated in cells.

Human natural killer-1 (HNK-1) carbohydrate is highly expressed on several cell adhesion molecules in the nervous system, including the neural cell adhesion molecule (NCAM) (7, 8). HNK-1 carbohydrate has a unique structure, including a sulfated trisaccharide (HSO_3-3GlcAβ1–3Galβ1–4GlcNAc-) (9, 10), and is biosynthesized by the successive actions of β-1,4-galactosyltransferase (β4GalT), a glucuronyltransferase (GlcAT-P or GlcAT-S), and a sulfotransferase (HNK-1ST) (11–13). We previously generated mice lacking the gene for GlcAT-P, a major glucuronyltransferase in the nervous system (14). The GlcAT-P-deficient mice showed an almost complete loss of HNK-1 expression in the brain and exhibited reduced long term potentiation at hippocampal CA1 synapses along with impaired maturation of dendritic spines, indicating an important role for this glycan in synaptic plasticity (14, 15). In terms of the expression, we have been uncovering well controlled mechanisms of HNK-1 biosynthesis. For instance, GlcAT-P (S) and HNK-1ST form a functional complex, and the distribution of GlcAT-P in the Golgi is regulated by a small GTPase (16). However, it is still unclear how the inner *N*-acetyllactosamine structure (Galβ1–4GlcNAc) for HNK-1 carbohydrate is synthesized and how HNK-1 is selectively attached to limited kinds of carrier proteins.

* This work was supported in part by Grant-in-aid for Scientific Research (B) 21370053 (to S. O.) from the Ministry of Education, Culture, Sports, Science and Technology and in part by the Ministry of Health, Labor, and Welfare of Japan Health and Labour Sciences Research Grant on Comprehensive Research on Disability Health and Welfare, H21-012.

[S] The on-line version of this article (available at http://www.jbc.org) contains supplemental Figs. 1–3.

[1] Present address: Disease Glycomics Team, Systems Glycobiology Research Group, Advanced Science Institute, RIKEN, Saitama 351-0198, Japan.

[2] To whom correspondence should be addressed: Kawahara-cho 53, Shogoin, Sakyo-ku, Kyoto 606-8507, Japan. Tel./Fax: 81-75-751-3959; E-mail: shogo@hs.med.kyoto-u.ac.jp.

[3] The abbreviations used are: ER, endoplasmic reticulum; β4GalT, β1, 4-galactosyltransferase; GlcAT, glucuronyltransferase; HNK-1, human natural killer-1; PSA, polysialic acid; PST, polysialyltransferase; NCAM, neural cell adhesion molecule; ASOR, asialo-orosomucoid.

Although the β4GalT family is known to have seven members (β4GalT-I to VII) *in vivo* (17, 18), the biological role of each is not fully understood. Some of them are able to synthesize *N*-acetyllactosamine on glycoproteins. which is potentially further modified by GlcAT-P. We recently reported that β4GalT-II-deficient mice showed similar phenotypes to GlcAT-P-deficient mice with a reduction in HNK-1 expression and impaired spatial learning and memory (19), although HNK-1 expression was unaltered in the β4GalT-I-deficient mouse brain (20) despite the similarity in primary structure and acceptor specificity of these two enzymes (21, 22). These results indicated that β4GalT-II has specific roles in the biosynthesis of HNK-1 carbohydrate. However, the precise molecular mechanism has not been explored.

Polysialic acid (PSA), a well known neural specific glycan, plays crucial roles in the development of the nervous system, attenuating cellular interactions because of its large and highly negative charge (23, 24). PSA has features in common with HNK-1 in that it is mainly expressed on NCAM and has an *N*-acetyllactosamine residue (Galβ1–4GlcNAc-) in its backbone structure synthesized by β4GalT (25). Surprisingly, however, β4GalT-II-deficient mice as well as β4GalT-I-deficient mice expressed PSA at the same level as wild-type mice (19, 20), indicating the biosynthesis of HNK-1 and PSA to be more complicated mechanisms than was previously thought.

In this study, we demonstrated that β4GalT-II but not β4GalT-I physically interacts with GlcAT-P but not with a polysialyltransferase (PST), which explains the loss of or remaining expression of HNK-1 or PSA in these knock-out mice. Furthermore, overexpression of β4GalT-II enhanced HNK-1 biosynthesis by GlcAT-P compared with β4GalT-I, suggesting that β4GalT-II is specifically required for production of HNK-1.

EXPERIMENTAL PROCEDURES

Materials—The monoclonal antibody (mAb) M6749 against HNK-1 carbohydrate was a gift from Dr. H. Tanaka (Kumamoto University). HNK-1 mAb was purchased from the American Type Culture Collection. The rat anti-mouse NCAM mAb (clone H28) was kindly provided by Dr. K. Ono (Kyoto Prefectural University). RCA120 was purchased from Seikagaku Corp., Tokyo, Japan. The mouse anti-FLAG M2 mAb and rabbit anti-FLAG polyclonal antibody (pAb) were obtained from Sigma. The mouse anti-Myc mAb and rabbit anti-Myc pAb were from Millipore and Abcam, respectively. The rabbit anti-GlcAT-P pAb (GP2) was generated as described previously (16). The mouse anti-GM130 mAb was purchased from BD Biosciences. HRP-conjugated anti-mouse IgG, anti-mouse IgM, anti-rabbit IgG, and anti-rat IgG were obtained from Invitrogen. Protein G-Sepharose TM4 Fast Flow and IgG-Sepharose TM6 Fast Flow were from GE Healthcare. The expression vector pcDNA3.1/myc-His B was from Invitrogen, and p3×FLAG-CMV-10 and p3×FLAG-CMV-14 were from Sigma. The plasmid pEF-BOS was kindly provided by Dr. S. Nagata (Kyoto University).

Mice—β4GalT-I-deficient mice and β4GalT-II-deficient mice were generated as described previously (19, 26). β4GalT-II-deficient mice backcrossed to C57BL/6 mice for more than 10 generations were used for the experiments, whereas β4GalT-I-deficient mice on a mixed background of 129/Sv and C57BL/6 were used because the mice with the C57BL/6 background were lethal.[4] The animal experiments were conducted according to the Fundamental Guidelines for Proper Conduct of Animal Experiments and Related Activities in Academic Research Institutions under the jurisdiction of the Ministry of Education, Culture, Sports, Science and Technology of Japan and approved by the Committees on Animal Experimentation of Kanazawa University and Kyoto University.

Preparation of Brain Homogenate and Membrane Fraction—Whole brains from 4-week-old mice were homogenized with a Polytron homogenizer in 9 volumes of 50 mM Tris-HCl, pH 7.4, containing 150 mM NaCl, 1 mM EDTA, and protease inhibitors (Nacalai Tesque, Kyoto, Japan). The homogenate was centrifuged at 1,000 × *g* for 10 min at 4 °C to remove the nuclei and then centrifuged again at 105,000 × *g* for 1 h at 4 °C. The resulting pellet was used as the membrane fraction.

Peptide N-Glycosidase F Digestion—The membrane fraction of mouse brain was dissolved and denatured with phosphate-buffered saline (PBS) containing 0.5% SDS, 1% 2-mercaptoethanol, and 20 mM EDTA. To reduce the concentration of SDS, the sample was diluted with 4 volumes of PBS containing 0.5% Triton X-100. Two units of peptide *N*-glycosidase F (Roche Applied Science) were added, and the solution was incubated for 16 h at 37 °C.

Expression Plasmids—The subcloning of rat GlcAT-P cDNA into pEF-BOS was performed as described previously (11). The expression plasmid for GlcAT-P-AAA (pEF-BOS/GlcAT-P-AAA) was constructed as reported (16). The mouse β4GalT-I and β4GalT-II coding sequences were amplified by PCR using the primers listed below to create HindIII and EcoRV (skipping stop codon) sites and then cloned into pcDNA3.1/myc-His B. The mouse PST coding sequence was cloned into p3×FLAG-CMV-14 as described previously (16). The expression plasmid for PST-AAA-FLAG (p3×FLAG-CMV-14/PST-AAA) was constructed as follows. p3×FLAG-CMV-14/PST-AER-FLAG was constructed using QuikChange Lightning site-directed mutagenesis kits (Stratagene) according to the manufacturer's directions using the primers listed below, with p3×FLAG-CMV-14/PST-FLAG as a template. Then, p3×FLAG-CMV-14/PST-AAA-FLAG was constructed as mentioned above using the primers listed below, with p3×FLAG-CMV-14/PST-AER-FLAG as a template. cDNAs encoding the Golgi luminal domains of mouse β4GalT-I and -II (from Ser-43 and Asp-33 to the C terminus) were amplified by PCR using the primers listed below and cloned into pEF-BOS-protein A (27), which contains the insulin signal sequence and IgG-binding domain of protein A. For the constructions of prot.A-GalT-Icat and -IIcat, cDNAs encoding the catalytic domains of mouse β4GalT-I and -II (from Leu-128 and Ile-91 to the C terminus) (28) were amplified by PCR using the primers listed below and cloned into pEF-BOS-protein A. pEF-BOS-protein A was digested with SmaI. Then the blunt end fragments of β4GalTs were cloned. GlcAT-P-sol was amplified by PCR using the primers listed

[4] M. Asano and N. Hashimoto, unpublished results.

below with pEF-BOS/GlcAT-P as a template to create EcoRV and NotI sites, and cloned into pEF-1/V5-His A into which the signal sequence of insulin had been inserted between EcoRI and EcoRV sites.

The primers used for β4GalT-I-myc were as follows: GGGAAGCTTGCGGGCCGTCCTCTCAGCCG and TCTCGGTGTCCCGATGTCCACTGTG; β4GalT-II-myc, GGGAAGCTTCTTGCGGGATGAGCAGACTG and GCCTTGAGTGAGCCACGAGA; PST-AER-FLAG, ATGCGCTCAATTGCAGAACGGTGGACCATCTGCACTATAAGTC and GACTTATAGTGCAGATGGTCCACCGTTCTGCAATTGAGCGCAT; PST-AAA-FLAG, ATGCGCTCAATTGCAGCAGCGTGGACCATCTGCACTATAAGTC and GACTTATAGTGCAGATGGTCCACGCTGCTGCAATTGAGCGCAT; prot.A-GalT-I (Ser-43), CTGGCCGCGATCTGAGCCG and CTATCTCGGTGTCCCGATGTCCACT; prot.A-GalT-II (Asp-33), ACGTCTATGCCCAGCACCTGG and TCAGCCTTGAGTGAGCCACGACATG; prot.A-GalT-Icat (Leu-128), TGCCAGCTTGCCCTGAGGAG and CTATCTCGGTGTCCCGATGTCCACT; prot.A-GalT-IIcat (Ile-91), TCATTCCGCCCTGTCCTGAC and TCAGCCTTGAGTGAGCCACGACATG; and GlcAT-P-sol, CCCCGCCATGAGGCACCACC and TGAGCGGCCGCTCAGATCTCCACCGAGGGGT.

Cell Culture and Transfection—N2a cells were cultured in minimum Eagle's medium supplemented with 10% fetal bovine serum at 37 °C until 50–70% confluent. For transfection, cells were plated on 60-mm tissue culture dishes, grown overnight, and then transfected with various expression constructs using FuGENE 6 (Roche Applied Science) according to the manufacturer's directions. Briefly, a 2.5 volume of FuGENE 6 and 1 μg of each DNA were incubated with 100 μl of minimum Eagle's medium for 15 min at room temperature, and then the mixture was added to the tissue culture dishes.

Cell Lysis and Immunoprecipitation of Transiently Expressed Proteins—Cells were collected 24 h after transfection and lysed with a buffer consisting of 20 mM Tris-HCl, pH 7.4, 150 mM NaCl, 1 mM EDTA, 1% Triton X-100, and a protease inhibitor mixture (Nacalai Tesque). After centrifugation, the clarified lysate was incubated with the anti-FLAG rabbit pAb or anti-Myc rabbit pAb for 0.5 h. The mixture was then incubated with protein G-Sepharose TM4 Fast Flow for 2 h with gentle shaking. The beads were precipitated by centrifugation (500 × *g* for 1 min) and washed three times with an excess volume of wash buffer consisting of 20 mM Tris-HCl, pH 7.4, 150 mM NaCl, and 0.1% Tween 20. Proteins bound to the Sepharose beads were eluted by boiling in Laemmli sample buffer.

Immunostaining of N2a Cells—At 24 h post-transfection, cells were washed with PBS, fixed with ice-cold methanol, and incubated with primary antibodies followed by Alexa Fluor-conjugated secondary antibodies (Invitrogen). Cells were visualized with a Fluoview laser confocal microscope system (Olympus).

SDS-PAGE and Western Blot and Lectin Blot Analyses—Proteins were separated by SDS-PAGE with the buffer system of Laemmli and transferred to nitrocellulose membranes. For Western blotting, after being blocked with 5% skim milk in PBS containing 0.05% Tween 20, the membrane was incubated with primary antibodies followed by HRP-conjugated secondary antibodies. For lectin blotting, after being blocked with PBS containing 0.05% Tween 20 (T-PBS), the membrane was incubated with sialidase (Roche Applied Science) according to the manufacturer's instructions, and then incubated with HRP-conjugated lectin in T-PBS. Protein bands were detected with ECL (Pierce) using a LAS3000 Luminoimage analyzer (Fujifilm).

Pulldown Assays—N2a cells were transiently transfected with prot.A-GalT-I (Ser-43), -Icat (Leu-128), -II (Asp-33), or -IIcat (Ile-91) and GlcAT-P-sol. After 6 h of incubation, the culture medium was replaced with serum-free Opti-MEM I (Invitrogen) and incubation continued for another 2 days. Normal human IgG-conjugated Sepharose beads were added to the culture medium containing secreted proteins. The beads were precipitated by centrifugation (500 × *g* for 1 min) and then washed three times with an excess volume of wash buffer consisting of 20 mM Tris-HCl, pH 7.4, 150 mM NaCl, and 0.1% Tween 20. Proteins bound to the Sepharose beads were eluted by boiling in Laemmli sample buffer.

Preparation of Protein A-fused GalTs—COS-1 cells plated on 175-cm^2 tissue culture flasks were transfected with prot.A-GalT-I (Ser-43) or prot.A-GalT-II (Asp-33) using FuGENE 6 transfection reagent. After 5 h of incubation, the culture medium was replaced with serum-free ASF104 medium (Ajinomoto), followed by incubation for another 3 days. Then, the culture medium containing secreted proteins was applied to IgG-Sepharose TM6 fast flow column (GE Healthcare). Unbound proteins were washed out with more than 10 column volumes of PBS. Bound proteins were eluted with 100 mM glycine-HCl, pH 2.5, and then the eluate was immediately neutralized with 3 M Tris-HCl, pH 8.0. The purified prot.A-GalTs were used for the following kinetic analysis of GlcAT-P.

Measurement of Glucuronyltransferase Activity—The FLAG-tagged GlcAT-P catalytic domain (FLAG-P) used was expressed in *Escherichia coli* and purified as described previously (29). The enzymatic activity of GlcAT-P toward glycoprotein acceptors was measured according to the procedure described previously (10) with slight modification. In brief, prior to the assay, FLAG-P (25 ng) was incubated in the absence or presence of prot.A-GalT-I (Ser-43) or prot.A-GalT-II (Asp-33) (100 ng each) at room temperature for 15 min. The preincubated enzyme solution was added to a reaction mixture with a final volume of 25 μl consisting of 200 mM MES, pH 6.5, 0.2% Nonidet P-40, 20 mM $MnCl_2$, 0.1–20 μg ASOR, 100 μM UDP-[^{14}C]GlcA (100,000 dpm), and 0.5 mM ATP. After incubation at 37 °C for 2 h, the assay mixture was spotted onto a Whatman No. 1 filter paper. The filter paper was washed with a 10% (w/v) trichloroacetic acid solution three times, followed by with ethanol/ether (2:1, v/v), and then with ether. The filter paper was air-dried, and then the radioactivity of [^{14}C]GlcA-ASOR was counted with a liquid scintillation counter.

RESULTS

Unaltered Expression of N-Acetyllactosamine on a Major HNK-1 Carrier in β4GalT-II-deficient Mice—Recently, we reported that HNK-1 expression is substantially reduced in β4GalT-II-deficient mice, although an earlier study revealed that β4GalT-I-deficient mice expressed normal levels of